Progress of 3D Network Binders in Silicon Anodes for Lithium Ion Batteries

Journal:	*Journal of Materials Chemistry A*
Manuscript ID	TA-REV-08-2020-007713.R1
Article Type:	Review Article
Date Submitted by the Author:	16-Oct-2020
Complete List of Authors:	Preman, Anjali; Pusan National University, Polymer Science and Engineering Lee, Hyocheol ; Pusan National University, Polymer Science and Engineering Yoo, Jungwoo ; LG Chem Daejeon, Advanced Automotive Battery Development Center Kim, Il Tae; Gachon University, Chemical and Biological Engineering Saito, Tomonori; Oak Ridge National Laboratory, Chemical Sciences Division Ahn, Suk-kyun; Pusan National University, Polymer Science and Engineering

SCHOLARONE™
Manuscripts

Progress of 3D Network Binders in Silicon Anodes for Lithium Ion Batteries

Anjali N. Preman[a], Hyocheol Lee[a], Jungwoo Yoo[b], Il Tae Kim[c,*], Tomonori Saito[d,*], Suk-kyun Ahn[a,*]

Prompted by its overwhelming benefits, silicon (Si) has evolved as one of the most promising anode materials for high-capacity lithium-ion batteries (LIBs). However, some of the intrinsic drawbacks such as low ionic conductivity and inevitable volume change during the alloying/dealloying process seriously hamper the commercialization of Si-based anodes in LIBs. Among the several strategies to overcome the challenges of the Si anode, the development of designed polymeric binders is imperative for enabling stable and satisfactory performance. The improved cell performance by designed binders is recognized as an economical and practical approach, especially from the industrial perspective. In addition to their conventional role as integrating electrode components, binders also play a significant role in alleviating the unfavorable phenomenon of volume expansion, and ultimately stabilizing the Si anode and Si-electrolyte interphase. The polymer architecture of the binders significantly influences the binder performance, and three-dimensional (3D) network binders are generally more effective at coping with the stress resulting from the huge volume change of the Si anode. To develop advanced 3D binders, substantial research efforts have been devoted including various crosslinking strategies in the past decade. In this review, we focus on the diverse crosslinking methods including chemical-, physical-, and topological-crosslinking for rationally designed network binders for Si anodes and a glance into dynamic interactions to construct healable binders for long-term stability.

Keywords: polymer binder, lithium-ion batteries, silicon anode, crosslinking

1. Introduction

The alarming increase in greenhouse gas emissions and global warming compelled both governments and industries to constantly explore alternatives to fossil fuels. Although wind, thermal, and geothermal energy offer renewable energy solutions, their minimal energy density is insufficient to satisfy the ever-growing energy demands.[1,2] Being the largest consumer of fossil fuels, the automobile industry holds significant influence in revolutionizing the energy landscape of the electric power sector. Lithium-ion batteries (LIBs) represent an excellent energy storage system by providing high energy densities.[3-6] Owing to their small size, lithium ions can easily travel in the electrolyte between the anode and cathode, providing a high voltage, charge storage per unit volume (700 Wh l^{-1}), and unit mass (260 Wh kg^{-1}).[7,8]

Apart from powering a range of portable electronic devices, such as mobile phones and laptops, LIBs have enabled a radical transfiguration of electric vehicles (EV) and hybrid electric vehicles (HEV).[9] However, the performance of conventional LIBs is still limited and cannot satisfy the requisites of vehicle electrification on a large scale.[4,10] To realize the concept of all-electric vehicles powered by LIB for long-distance travel (> 500 km), next-generation LIBs with higher energy densities (> 350 Wh kg^{-1} at cell level) must be developed.[8,11,12] For this reason, researchers have been continuously seeking a new class of anode materials such as silicon (Si), which generate a high capacity to replace the conventional graphite anodes. Si possesses various characteristics that are superior to those of graphite and other candidate materials (e.g., S, Sn, and Ge), including a high theoretical capacity (3579 mAh g^{-1} for $Li_{15}Si_4$) and low working voltage (~ 0.4 V vs Li/Li$^+$), as well as resource abundance (28.2% in earth crust) and harmless nature.[13-16]
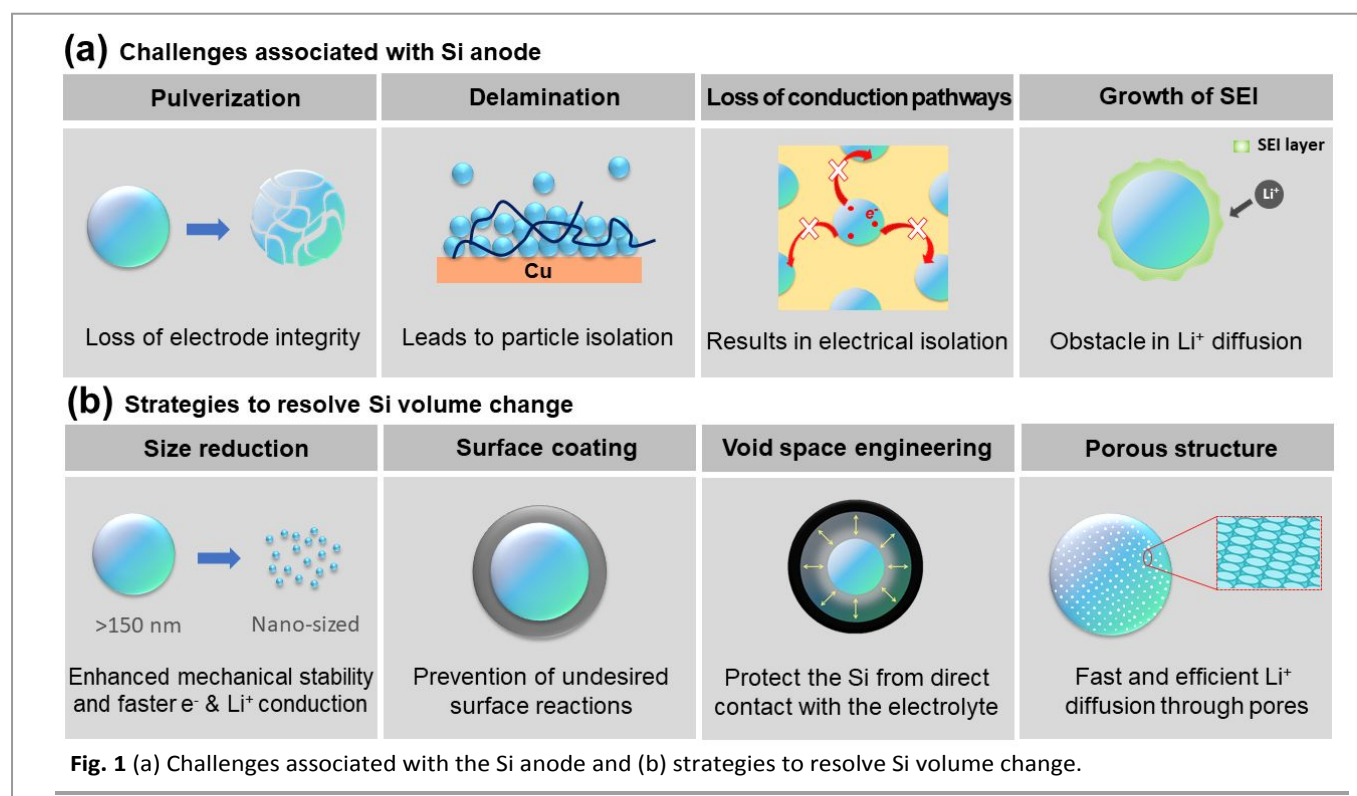
Despite these benefits, Si-based anodes suffer from chronic capacity decay, predominantly due to pulverization and delamination of the Si particles and continuous growth of the solid-electrolyte interlayer (SEI) (Fig. 1a)[10,15,17,18]. SEI is an electronically passive layer formed by an unavoidable reduction of the electrolyte at the surface of the electrode. This thin layer allows Li-ions to penetrate back and forth while protecting the electrode surface from further exposure to the electrolyte.[19,20] However, this SEI layer continues to grow in the Si-based anodes until it becomes hard and eventually collapses.[21,22] The

a. Department of Polymer Science and Engineering, Pusan National University, Busan 46241, Republic of Korea. E-mail: skahn@pusan.ac.kr
b. Advanced Automotive Battery Development Centre, LG Chem, Daejeon, 34122, Republic of Korea
c. Department of Chemical and Biological Engineering, Gachon University, Seongnam-si, Gyeonggi-do 13120, Republic of Korea. Email: itkim@gachon.ac.kr
d. Chemical Sciences Division, Oak Ridge National Laboratory, Oak Ridge, Tennessee 37831, United States. Email: saitot@ornl.gov

Fig. 1 (a) Challenges associated with the Si anode and (b) strategies to resolve Si volume change.

main cause of these events is associated with the immense volume expansion of Si (≈300%) during the alloying process. Unlike the graphite anodes consisting of a layered structure to accommodate the Li-ions between the layers (intercalation), Si anodes alloy with Li-ions to configure various phases of lithium silicates (Li_xSi).[23] Upon initial lithiation, the crystalline Si (c-Si) undergoes a phase transition to the amorphous form (a-Si) and preserves this phase for the rest of the cycle. Typically, each Si atom can store up to 4.4 Li atoms corresponding to a very high capacity at the cost of the undesirable volume changes.[24,25] Yan research group investigated the failure mechanism of the Si anode through simulations and real time nanoindentation measurements.[26] They postulated that the elastic modulus and hardness of amorphous Si undergo considerable reduction on full lithiation due to the breakdown of strong Si-Si bonds and formation of Si-Li and Li-Li bonds that are less directional, weak and more inclined to deformation.

To circumvent the consequences of the volume changes in Si, several strategies have been developed, such as engineered electrode structures by introducing nano,[27-29] porous,[30-34] and 3D architectures, which can cope with the stress resulting from volume expansion (Fig. 1b). Among them, shape-preserving designs such as core-shell, yolk-shell, and pomegranate-inspired designs have received considerable attention.[35-38] The most distinctive feature of these designs is the inclusion of confined voids for the Si particles to dilate. Nevertheless, high cost, reduced tap density, and low areal mass loading limit the practice of these design principles.[39]

Recently, it has been perceived that properly designed binders can substantially contribute to improving the cycle life of Si-based LIBs (Fig. 2). Despite used in small doses, binders play a decisive role in determining the electrochemical stability of the electrode and therefore the lifetime of the cells. Conventionally, the binder provides a crucial contribution in

Fig. 2 Response of various binders (linear, branched, and crosslinked) to Si volume change.
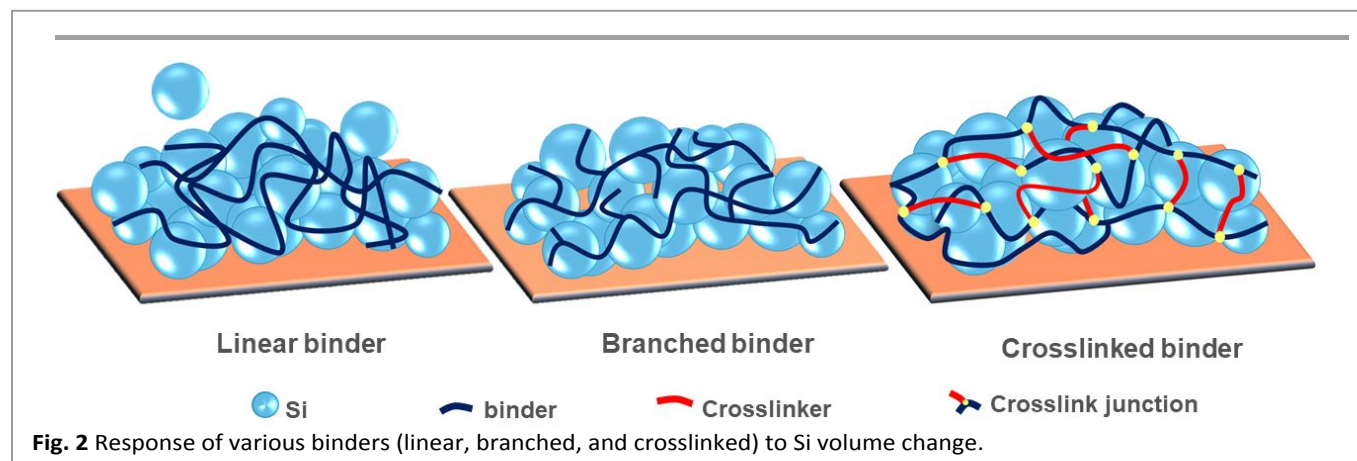
bridging the active materials together as well as in preserving the Li-ion conduction pathways, particularly at the electrode-electrolyte interphase.[40] In addition to this conventional role, polymeric binders in alloy-based LIBs also buffer the stress caused by volume expansion. To alleviate the effects of undesired events during cycling, binders should possess robust cohesion and adhesion properties. Specifically, sturdy interactions with both the active materials as well as the current collector are critical for the binders to hold the particles in place under stress. The electrolyte influences the wetting and swelling properties of binder, which affects the electrode stability and ion transport. In general, the binders are encouraged to show adequate wettability to promote the electrolyte diffusion and Li-ion transport, while swelling, on the other hand, should be minimal not to hamper the interactions between the binder and the electrode components. Strategies for designing an efficient binder also include (i) availability and economical processing, (ii) chemical stability at elevated temperatures and electrochemical stability to satisfy wide electrochemical window, (iii) mechanical durability to withstand extensive stresses, (iv) self-healing or shape-memory properties, and (v) preservation of ionic or electronic conduction.[1,41]

Poly(vinylidene fluoride) (PVDF) is the standard binder for LIBs with carbonaceous anodes due to its electrochemical stability, binding ability, and enhanced Li-ion transportation. However, PVDF is not suitable for alloy-based anodes because of the weak interactions with the active materials and the current collector, which leads to an unstable electrode during drastic volume changes.[42] The presence of polar functional groups (e.g., -OH, -COOH, -(C=O)NH$_2$) in the polymer is important when designing a "better binder" for Si anodes because they can strongly interact with the silanol groups on the Si surface as well as encourage the dissolution of the binder in the solvent for facile processing.[43] To this end, several natural (e.g., gelatin,[44] carboxymethyl cellulose (CMC),[45] alginate,[46] pectin[47] etc.) and synthetic polymers (e.g., poly(acrylic acid) (PAA),[48] poly(vinyl alcohol) (PVA),[49,50] polyacrylonitrile (PAN)[51] etc.) have been extensively explored, and found to be effective for enhancing the cyclability of Si,[42] Si/C, and Si/Gr composite anodes.[52,53] However, one-dimensional configuration of these binders is fundamentally limited in interaction with the Si surface and is insufficient to restrain the swelling in the electrolyte.[54,55] Branched polysaccharides such as gum arabic ,[56] xanthan gum ,[57] and graft copolymers including NaPAA-g-CMC,[58] PAL-NaPAA,[59] and PVDF-g-PtBA[60] etc. have been also investigated to provide more contact points with the active materials, which could be beneficial for effective stress-dissipation. Nonetheless, the slipping of the polymer chains during volume expansion still occurs due to the lack of interchain connections, which challenges the long-term stability of the electrode.

3D polymer networks have been developed to surpass the linear and branched polymers.[61-63] Network binders offer multiple interchain connections that strengthen the mechanical integrity to withstand the immense stress generated during cycling. The interconnected architecture in the network binders can be formed by covalent interactions[64,65] as well as non-covalent interactions (e.g., hydrogen bonding and electrostatic interactions).[66,67] Covalent crosslinking offers the advantage of an in-situ strategy, where the crosslinks result from heat treatment or light exposure to the precursor polymers. The approach with network polymers possessing supramolecular interactions is salient because they not only limit the continuous movement of Si particles but also offer a self-healing effect.[68]

Recently, the self-healing properties of the binders have received considerable attention for battery applications. Self-healing is a natural process involving the subsequent formation and repair of damage with(out) the utilization of an external stimulus.[69] Extrinsic healing induced by specific stimuli is often difficult to achieve in sophisticated and closed systems, such as energy storage devices.[70] Therefore, intrinsic self-healing through reversible or dynamic bonds is more appealing. Based on the nature of the dynamic bonds, the mechanism can be physical or chemical self-healing.[71] The healing process not only replicates the pristine structure of the binder but also intensifies the overall efficacy of the cell by re-establishing the conduction pathways and mechanical resilience.

Excellent review articles have been published highlighting the role of polymeric binders in LIBs[68,72] and their classification based on source, processing media, etc.[73] Although some of these articles have briefly discussed the crosslinking chemistries, an in-depth investigation of all the strategies (both physical and chemical) and bonding chemistries is not available. In this review, we present a comprehensive survey of the crosslinked binders reported to date and provide insights to a variety of crosslinking chemistries, including dynamic interactions to realize the self-healing effect. The cited literature has been scrutinized to identify the impact of 3D networks on the electrochemical stability of Si anodes.

2. Covalently crosslinked binders

Considering the fact that covalent bonds possess high dissociation energies and therefore are not easily broken, covalent crosslinking chemistry is well-suited in binder technology for the Si anode. Most of the covalently crosslinked binders are formed by an in-situ condensation reaction between the reactive functional groups of the precursors during the electrode drying process. This post-crosslinking approach overcomes the problem of low solubility of the crosslinked binders and simplifies electrode processing. The majority of the prominent binders such as PAA, polyacrylamide (PAAm), PVA, and linear and branched polysaccharides have been extensively explored for covalent crosslinking to consolidate the Si particles under stress. Similarly, several in-situ condensation reactions such as esterification and the Schiff-base reaction have been successfully employed. For a better understanding, we classify the covalently crosslinked binders based on the type of crosslinking reactions (Fig. 3 and Table 1).

Table 1 Summary of covalently crosslinked binders reviewed herein. For the chemical structure of each binder, please see the discussion part or the relevant references.

Binder	Anode (mass loading in mg cm^{-2})	Crosslinking reaction	Specific capacity (mA h g^{-1})	Binder content (wt%)	Capacity retention	Ref
c-PAA-CMC	Si = <100 nm (not mentioned)	In-situ condensation of -COOH of PAA and -OH of CMC @ 150 ˚C	~2800	20	~75% after 100 cycles at 0.3 A g^{-1}	74
PAA-co-PVA	Si = ~100 nm (not mentioned)	In-situ condensation of -COOH of PAA and -OH of PVA @ 150 ˚C	2153	20	not mentioned	78
PAA-PVA Hydrogel	Si = 30-100 nm (<1.0)	In-situ condensation of -COOH of PAA and -OH of PVA @ 150 ˚C	3616	20	63% after 100 cycles at 0.4 A g^{-1}	79
PAA-Pullulan	Si = ~100 nm (not mentioned)	In-situ condensation of -COOH of PAA and -OH of PVA @ 150 ˚C	2493	20	78% at 200th cycle at 0.5 C	81
PVTES-NaPAA	Si = 50-100 nm (~0.54)	Hydrolysis followed by condensation of ethyl silicate groups	2654	20	78.2% after 100 cycles at 0.84 A g^{-1}	82
PAA-GL	Si (SiO$_2$ coated) 50-100 nm (~0.5)	In-situ condensation of -COOH of PAA and -OH of GL @ 150 ˚C	~2400	10	82% after 200 cycles at 1.0 C	83
TBA-co-TEVS	Si (C coated) ~150 nm (~1.0)	In-situ condensation of -COOH groups @ 220 ˚C	~2500	15	>2000 mA h g^{-1} after 100 cycles at 0.5 A g^{-1}	84
PAA-PCD	Si/Gr = 3/5 (Si <100 nm, Gr 3 µm) (0.6)	Reaction of PAA and PCD to form N-acyl urea linkage @ 150 ˚C	~1000 at 0.1 A g^{-1}	10	75% after 30 cycles at 0.1 A g^{-1}	85
CS-GA	Si = ~100 nm (not mentioned)	Condensation between -NH$_2$ of chitosan and -CHO of glutaraldehyde	2782 at 0.5 A g^{-1}	20	71% after 100 cycles	86
CS-CG-GA	Si = <100 nm (0.4)	Condensation between -NH$_2$ of chitosan and -CHO of glutaraldehyde	2345	20	91.5% after 100 cycles	87
c-PVA	Si = ~120 nm (not mentioned)	TMM as crosslinker (ex-situ)	3335	20	85% after 500 cycles at 0.8 A g^{-1}	88
PVA-PEI	Si = ~50 nm (1.8–2.7)	Condensation between -OH of PVA and -NH- of PEI	3073 at 1.0 A g^{-1}	20	72.2% at 100th cycle	43
DG	Si = ~100 nm (0.9)	Glutaraldehyde as crosslinker (ex-situ)	3276 at 0.4 A g^{-1}	20	63% after 50 cycles	90
CMC/PEG	Si = ~50 nm (0.4)	PEGDE as crosslinker (in-situ)	~2300	10	~78% from 3rd to 350 cycles at 1.7 A g^{-1}	91
p(AA-co-*n*BA)	Si = ~50 nm (0.55–0.68)	PEGDE as crosslinker (in-situ)	3050	15	40% after 100 cycles at 0.5 A g^{-1}	92
CE	Si = ~100 nm (0.6)	Epoxidized natural rubber as crosslinker	not mentioned	15	62% from 11th to 300th cycle at 8 A g^{-1}	93
PEU	Si = ~50 nm (0.55)	Gallic acid as crosslinker (in-situ)	3400 at 0.2 C	20	71% after 100 cycles	94
CLPAH	Si/Gr = 3/5 (Si <100 nm, Gr 3 µm) (0.6–1.0)	Di-allyl ether in the copolymer act as crosslinker	~1500 at 0.05 A g^{-1}	10	~800 mA h g^{-1} at 0.1 A g^{-1}	95
PAA-BP	Si = <100 nm (not mentioned)	Photo-crosslinking of PAA chains	~1600 at 0.1 A g^{-1}	20	1400 mA h g^{-1} after 100 cycles at 0.2 A g^{-1}	96

Table 1 continued.

Binder	Anode (mass loading in mg cm^{-2})	Crosslinking reaction	Specific capacity (mA h g^{-1})	Binder content (wt%)	Capacity retention	Ref
cPA	Si = ~2 μm (not mentioned)	In-situ polymerization of acrylic acid @ 72 °C	2542 at 0.2 A g^{-1}	10	80% after 100 cycles	97
PAM Hydrogel	Si = ~50 nm (~0.6)	In-situ polymerization of acrylamide and MBAA crosslinker @ 35 °C	~2543 at 0.7 A g^{-1}	20	~1526 mA h g^{-1} after 500 cycles	98
PFA/PVA-3D-IBN	Si = 100 nm (2.2)	In-situ polymerization of FA with PVA @ 140 °C	2916.5 at 0.1 A g^{-1}	20	2200 mA h g^{-1} at 1 A g^{-1} at 60th cycle	99

2.1. Esterification

The condensation of the carboxyl and hydroxyl groups to form an ester linkage is a versatile reaction to achieve network binders. Most of the well-known binders such as PAA, CMC, alginate (Alg), and PVA intrinsically contain these functional groups, and therefore can be easily crosslinked by choosing an appropriate combination of such binders or employing a crosslinker with complementary functional groups.

The scope of crosslinking PAA and CMC by esterification was first investigated by Koo et al. (Fig. 3a).[74] Both PAA and CMC are well-established candidates for the Si anode binder owing to the abundance of carboxylic groups that are able to interact strongly with the Si surface via hydrogen bonding. Bare PAA for binder applications was pioneered by the Yushin group.[48] In their work, they compared the performances of Si anodes with both PAA and CMC binders. Although PAA and CMC have similar mechanical properties (high elastic modulus) and swelling behavior in carbonate solvents (no or little swelling), the former is superior in retaining the capacity for prolonged cycles compared to the latter. Initially, it was presumed that this superior performance evolved from the relatively higher concentration of −COOH functional groups in PAA. A recent study by Parikh et al.[75] on the role of these binders on SEI formation revealed that PAA can promote the complete consumption of F$^-$ to configure a stable bilayer (inorganic inner layer and organic outer layer) at the interphase so that it is unavailable for decomposition in the subsequent cycles. This stabilization was enabled by the strong intermolecular hydrogen bonding of the −COOH functional group with F$^-$.

From a structural perspective, the CMC backbone is more rigid or practically brittle due to the β-pyranose linkages, while the hydrocarbon backbone in PAA is more flexible. Although CMC may not withstand the large stresses caused by volume expansion, in contrast to PAA, Dahn and co-workers reported that CMC can act as a surface modifier to improve the surface properties of Si particles.[76] This is the mainstay in integrating these polymers to generate a synergistic effect.[77] The crosslinked network was formed by the thermal condensation of −COOH of PAA and −OH of CMC. By controlling the PAA to CMC ratio, a sufficient amount of free carboxylic acid groups could be retained on the PAA backbone to form hydrogen bonds with the Si surface. The co-operative effect of PAA with CMC and the robustness of the crosslinked network enabled the PAA-CMC-Si anode (60 wt% Si, 20 wt% conductive agent, and 20 wt% binder) to deliver much higher capacities (>2000 mA h g^{-1}) and a good retention capacity (~75%) over 100 cycles at a current density of 300 mA g^{-1}.[74]

Jeena et al. synthesized a crosslinked multifunctional binder by covalently linking the −COOH of PAA with the −OH of PVA within PAA-co-PVA copolymers (Fig. 3a).[78] The Si electrodes were prepared with 60 wt% active material, 20 wt% conductive agent, and evaluated a series of binders (P1−P4; 20 wt%) containing different ratios of monomers (PAA:PVA = 33:67 for P1, 60:40 for P2, 71:29 for P3, and 75:25 for P4). In this copolymer series, PAA was responsible for adhesion, while PVA provided flexibility. The crosslinking synergistically improved the mechanical properties of the binders. The electrochemical characterization of these binders revealed that the P2-Si anode exhibited the highest performance among P1−P4. P2-Si could also deliver sustainable cycling at different current densities ranging from 0.1−10 C with a specific capacity above 1000 mA h g^{-1}. This is due to the optimum balance between PAA and PVA in P2 that facilitated the binder in achieving the desired flexibility and adhesion. The role of the chain networks in limiting the deformation of the Si anode was clearly unveiled when a PAA/PVA mixture and the linear polymers were investigated as controls. The values of specific capacity and initial columbic efficiency (ICE) of the Si anodes with these binders (2133 mA h g^{-1}; 77% for PAA/PVA, 2000 mA h g^{-1}; 79% for PAA, 2133 mA h g^{-1}; 81% for PVA and 927 mA h g^{-1}; 46% for PVDF) were comparatively lower than the P2-Si anode (2153 mA h g^{-1}; 89%).

Song et al. developed an interpenetrating gel polymer binder to evaluate the potential of PAA-PVA crosslinked polymers for Si anodes (Fig. 3a).[79] The binder design was inspired by the flexible 3D network of superabsorbent resins that can normally revert to the original state after losing the absorbed solvent.[80] Unlike the previous approach, which incorporated copolymers consisting of acrylic acid and vinyl alcohol, they utilized aqueous solutions of PAA and PVA (9:1) as precursors. The crosslinking was achieved by the simple in-situ condensation of the acid and alcohol functional groups of the precursors. The Si electrode with 60 wt% active material, 20

wt% conductive agent and 20 wt% PAA-PVA binder exhibited good cycling performance, even at high mass loadings (~4.3 mA h cm^{-2} for 2.4 mg cm^{-2}) and high current densities (1830 mA h g^{-1} corresponding to 68.6% of initial capacity after 300 cycles at 4 A g^{-1}). The high ICE (83.9%) of PAA-PVA-Si indicated high stability of the formed SEI, potentially due to the mechanical strength of the interpenetrating gel network.

Hwang et al. developed an elastic binder by chemically crosslinking the carboxylate group in PAA and hydroxyl group in pullulan (PAA:Pullulan = 1:1 wt%) (Fig. 3a).[81] Unlike other polysaccharides such as CMC or alginate that contains β-1,4 linkages, pullulan contains α-1,6 and α-1,4 linkages, providing higher chain flexibility. This flexibility arises from the ability of the α-linkages to switch between chair and boat conformations. On account of this conformational change and consequent flexibility, PAA/Pullulan could reversibly deform to a larger extent than PAA/CMC, indicated by the difference in the thickness increment of the corresponding Si electrodes after lithiation. Moreover, the mechanical integrity of the crosslinked network of PAA/Pullulan was sufficient to keep the particles together. The Si electrodes fabricated with 20 wt% of both the binders (mass loading ~0.8 mg cm^{-2}) exhibited good cyclability up to 100 cycles. However, post cycling results demonstrated that a stiffer PAA/CMC network could not withstand volume changes for a prolonged period, whereas the Si anode containing the more flexible PAA/Pullulan binder retained a considerable capacity (78%) even after 200 cycles.

Zeng et al. reported a poly(vinyltriethoxysilane) (PVTES)-NaPAA binder for the Si nanoparticle (SiNP) anode.[82] The crosslinked network was formed by the hydrolysis and subsequent condensation of the ethyl silicate groups of the PVTES-NaPAA copolymer (Fig. 3b). The electrochemical performance of the crosslinked binder was evaluated by fabricating a Si anode with 60 wt% active material (mass loading 0.5–1.3 mg cm^{-2}), 20 wt% conductive agent, and 20 wt% binder. Galvanostatic cycling tests indicated that the crosslinked binder was superior to the un-crosslinked NaPAA and other commonly studied binders with a capacity retention of 78.2% over 100 cycles (37.5% for NaPAA and 57.9% for CMC). Moreover, the adhesion strength of the crosslinked binder was much higher than those of the control binders as demonstrated by the 180˚ peel test. These results suggest that the 3D network and multiple contacts with the Si surface are effective in binding the active materials and conductive additives under stress.

In a recent study, Sun et al. proposed a facile strategy to improve the cycle life of the Si anodes by employing glycerol (GL) modified PAA binder along with a SiO$_2$ coating on the surface of SiNP (Fig. 3a).[83] The crosslinked PAA-glycerol (GL) was prepared by the simple condensation of –COOH on PAA and –OH from glycerol during electrode drying. Compared to conventional PAA or CMC binders, the modified PAA-GL exhibited a higher modulus and hardness indicating stronger mechanical properties. The crosslinked binder also manifested superior adhesion with an average peeling force of 6.44 N which is nearly four times higher than the force of linear PAA (1.69 N) and CMC (1.30 N). For electrochemical measurements, the electrodes were fabricated with partially oxidized SiNPs (80

wt%, mass loading 0.5 mg cm^{-2}), conductive additive (10 wt%), and binder (10 wt%). The capacity of the SiO$_2$-coated Si anode with the PAA-GL binder after 500 cycles was almost 83% of the initial capacity while the same electrode with PAA or CMC exhibited a much lower capacity and capacity retention.

2.2. Anhydride formation

After the successful development of the covalently crosslinked copolymer binder, Jeena et al. used a similar strategy (combining –COOH to afford anhydride crosslinks) to synthesize a series of copolymers of t-butyl acrylate and triethoxyvinylsilane (TBA-co-TEVS-n) (n = 0, 9, 21, 50 wt%) for SiNP anodes.[84] The crosslinked binder was prepared by the condensation reaction between two adjacent carboxylic acid groups, which were formed in-situ as a consequence of t-butyl group deprotection upon heating at 220 °C (Fig. 3c). Irrespective of the weight percentage, all TEVS containing binders exhibited a high cycling capacity (> 2300 mA h g^{-1}), which was attributed to the stable SEI formation evidenced by XPS results. The low intensity of the LiF peak indicated a reduced decomposition of the electrolyte. However, the Si anode with TBA-TEVS-21 showed the best result with a high specific capacity and retention. The superior binder performance of TBA-TEVS-21 after crosslinking was further supported by the nanoindentation tests where the modulus (from 2.3 to 7.6 GPa) and hardness (from 0.09 to 0.27 GPa) were significantly enhanced after crosslinking.

2.3. N-acylurea linkage

Han et al. examined crosslinked PAA for Si/Gr composite anodes (3/5 by weight) (Fig. 3d).[85] In this work, poly(carbodiimide) (PCD) was introduced to crosslink the PAA chains by forming *N*-acylurea linkages between carboxylic acid and the carbodiimide groups. To evaluate the optimum degree of crosslinking, the morphology of the electrodes with different amount of PCD (0–1.5 wt%) were evaluated by SEM. The electrodes with an appropriate amount of PCD (1.0 wt%) significantly improved the slurry condition while a small excess of the crosslinker (1.5 wt%) resulted in a non-uniform distribution due to gelation. The composite anode with optimally crosslinked PAA (with 1.0 wt% PCD) exhibited a high initial capacity (1000 mA h g^{-1}) and improved capacity retention (75% at 30 cycles) compared with those of the anode containing PAA alone, which further improved in the presence of electrolyte additives.

2.4. Schiff-base reaction

Apart from the usual crosslinking chemistries involving the carboxylic acid group, Chen et al. prepared a crosslinked binder using the Schiff-base reaction to combine chitosan (CS) with various amounts of the glutaraldehyde (GA = 1–5 wt%) crosslinker (Fig. 3e).[86] Si electrodes were prepared with 60 wt% active Si, 20 wt% conductive agent, and 20 wt% CS–GA. Electrode drying at 80 °C induced imine linkages between the CS molecules by condensing the amine groups of CS and dialdehyde groups of GA. This study opened new avenues for the development of novel binders using the Schiff-base reaction. The CS–GA network retarded the growth of thick SEI by spreading over the Si particles and subsequently blocking the

electrolyte from decomposing at the electrode surface. This favorable effect was observed until chitosan molecules were moderately crosslinked (up to 3%). Further increases in the crosslinking density rapidly declined the capacity of the anode because an excessive amount of the crosslinker made the binder brittle and reduced the fraction of free amine groups to bond with the Si surface.

To advance beyond the previously reported capacity limits, Cao et al. functionalized the CS–GA binder with a catechol group possessing wetness-resistant adhesion.[87] The SiNP anode with a catechol-grafted chitosan network (CS–CG+GA) demonstrated enhanced capacity (2144 mA h g–1) and capacity retention (91.5%) for over 100 cycles. The CG grafting density and the degree of crosslinking of GA were optimized at 10% and 6%, respectively. The improved capacity retention of the functionalized CS–GA network was due to the combined effects of the strong adhesion of catechol and the robustness of the crosslinked network. The study also demonstrated that both catechol grafting and crosslinking resulted in reduced flexibility of the polymer backbone for the resultant binder system, and identified that the end-to-end distance of the two adjacent crosslinking points should be no less than the persistence length of the backbone for efficient binding performance.

2.5. Etherification

PVA has been a well-explored binder for Si anodes owing to the capacity of the hydroxyl groups to form strong interactions with the active material as well as the current collector. Attempts to crosslink PVA with PAA and poly(ethylene imine) (PEI) have been reported.[43,79] To further enhance the electrode performance, Shan et al. crosslinked PVA chains with a trimethylol melamine (TMM) crosslinker (0.08 mol%) and developed a PVA hydrogel binder (Fig. 3f).[88] The TMM crosslinker was prepared by the addition of melamine to formaldehyde followed by pH control with an appropriate amount of NaOH and vigorous agitation at 85 °C. The crosslinking was established by the condensation of the

Fig. 3 Chemically crosslinked binders and the corresponding crosslinking chemistry.
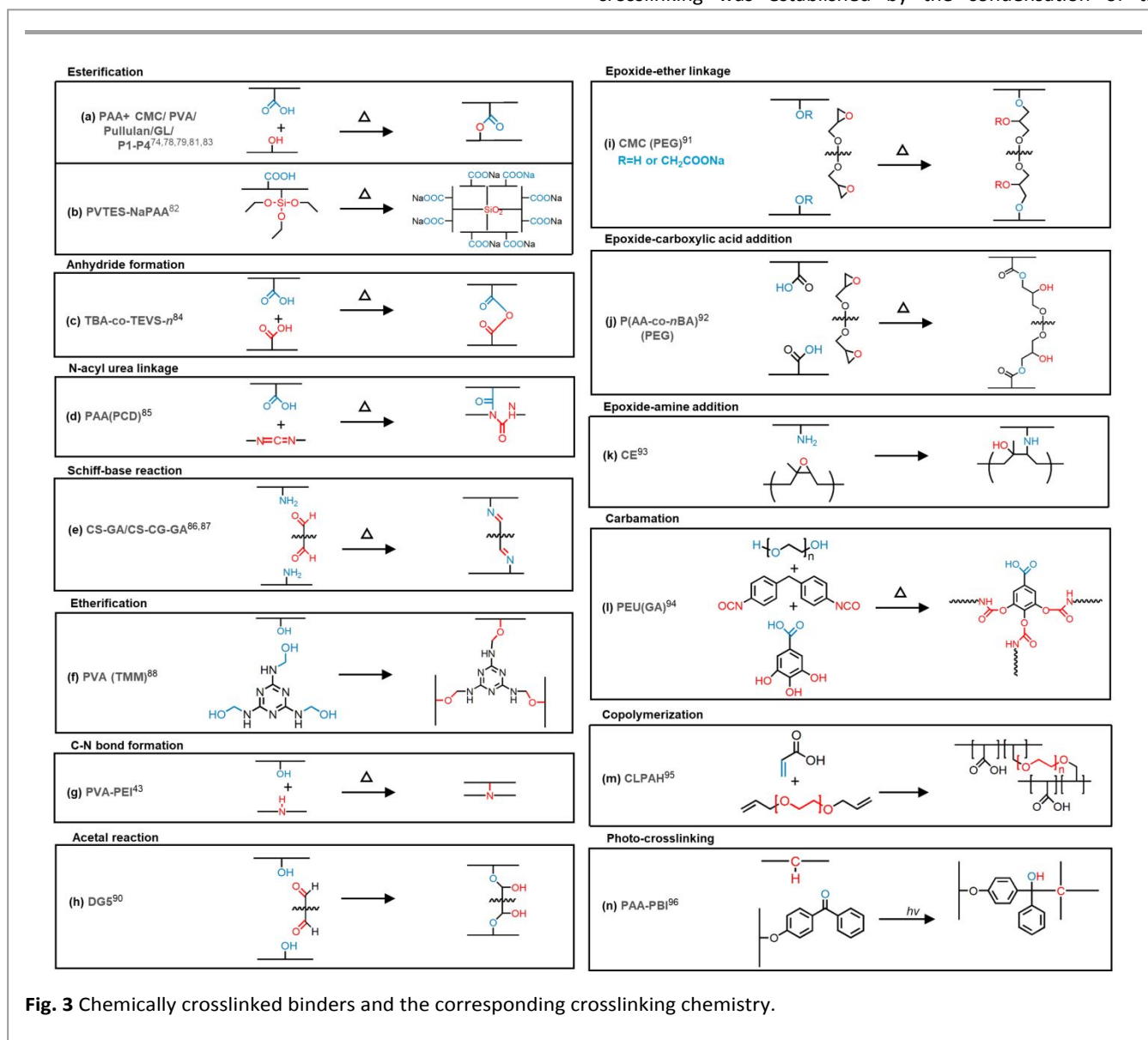
hydroxymethyl groups of TMM with the hydroxyl moieties of the PVA chains. The TMM crosslinker contains three hydroxymethyl groups which can simultaneously link with three hydroxyl groups of PVA, consequently generating a triple crosslink junction. The corresponding Si anode (Si:Super P:binder = 7:1:2) exhibited high mechanical integrity and excellent electrochemical stability (85% capacity retention over 500 cycles). Compared to the previously reported PVA-based electrodes, the Si anode with this unique binder demonstrated a high rate capability (3000 mA h g^{-1} at 20 °C). This refinement in overall performance can be attributed to the robustness of the triple crosslinked network that easily accommodates large stresses and the decreased impedance potentially due to enhanced ion conduction by the nitrogen groups of the crosslinker

2.6. C–N bond formation

Liu et al. reported a crosslinked binder formed by the condensation between the hydroxyl groups of PVA and the amine groups of PEI (Fig. 3g).[43] The PVA-PEI crosslinked network binder (8:2 by weight) was mixed with SiNP and a conductive agent in a weight ratio of 6:2:2 to evaluate the electrochemical performance. The corresponding Si anode (mass loading 1.8–2.7 mg cm^{-2}) exhibited a high initial capacity (3072.9 mA h g^{-1}) corresponding to an ICE of 83.8%. The high initial capacity and coulombic efficiency can be attributed to the initial stabilization of the SEI as demonstrated by the AFM results. Although it showed relatively good capacity retention (72.2%) at the 100th cycle, the long-term cycling stability gradually decreased to 41.3% after 300 cycles, indicating that the PVA-PEI binder required further improvement to address the long-term stability issue.

2.7. Acetal reaction

GA is also well-known for protein immobilization by crosslinking with proteins through a variety of reactions.[89] Chen et al. exploited the hydroxyl groups of dextrin (a decomposition product of starch with better water solubility) and the aldehyde groups of GA under acidic conditions to develop a crosslinked binder (DG) (Fig. 3h).[90] The electrode was fabricated with 60 wt% SiNP (mass loading 0.9 mg cm^{-2}), 20 wt% conductive agent, and 20 wt% binder. Owing to the presence of a large number of hydroxyl groups on the dextrin backbone, this natural polymer can form abundant interactions with the Si surface. The mechanical robustness of the binder-Si scaffold was further increased by interchain crosslinking evidenced by the peel test results of dextrin-containing Si anodes. The Si anode with the crosslinked binder exhibited a high initial capacity (3276 mA h g^{-1} at 0.1 C) and columbic efficiency (89%). However, the performance gradually declined for the Si anodes even in the presence of electrolyte additives (FEC).

2.8. Epoxide-ether linkage

Lee et al. crosslinked CMC using polyethylene glycol diglycidyl ether (PEGDE) to yield a three-dimensionally inter-connected CMC network (Fig. 3i).[91] During the electrode drying process, the carboxylate group of CMC reacted with the epoxide group of PEGDE to form ether linkages. The Si electrodes were prepared by combining 85 wt% Si (mass loading 0.4 mg cm^{-2}), 5 wt% conducting agent, 6.4 wt% CMC, 1.6 wt% PEGDE, and 2 wt% SBR. Despite the low content of PEGDE (25 % compared to CMC), the mechanical properties of the crosslinked network exhibited a remarkable improvement with good elastic recovery, reduced swelling ratio, and enhanced peel strength. In addition, the electrochemical tests revealed an enhancement of the capacity for the crosslinked CMC anode, as compared to the non-crosslinked CMC. The CMC-PEG-Si anode provided stable cycling with a high capacity of 2000 mA h g^{-1} (~78% retention) up to 350 cycles. These results clearly point out the role of PEG in reducing the stiffness of the CMC backbone by the plasticizing effect and in decreasing the charge-transfer resistance at the interface, as demonstrated by the nanoindentation and EIS results, respectively.

2.9. Epoxide-carboxylic acid addition

Recently, Ahn and coworkers reported a series of random copolymer binders consisting of acrylic acid and n-butyl acrylate, p(AA-co-nBA), crosslinked by PEGDE (Fig. 3j).[92] A systematic investigation by varying the composition of n-BA (10–70 mol%) and PEGDE crosslinker suggested that p(AA$_{70}$-co-nBA$_{30}$) with 14 wt% crosslinker can effectively alleviate the stresses of volume expansion and maintain the integrity of the electrode. As demonstrated by the linear viscoelastic measurements, the elastic moduli of the crosslinked binders gradually decreased with increasing crosslinking densities due to an increase in the internal plasticizing effect by the PEGDE crosslinker. The galvanostatic cycling test of the Si anodes (70 wt% SiNPs, mass loading 0.55–0.68 mg cm^{-2}) with 15 wt% binder indicated that moderately crosslinked random copolymer binders p(AA$_{70}$-co-nBA$_{30}$)-x (x = 5–14 wt%) exhibited superior cyclability compared to the non-crosslinked binder with the same composition. At 0.5 C, p(AA$_{70}$-co-nBA$_{30}$)-14 outperformed all the other binders, with a capacity retention of 40% after 100 cycles. It is noteworthy that the use of PEGDE crosslinker effectively improved the Li-ion conduction which is evident from the decreased internal resistance in the EIS results.

2.10. Epoxide-amine addition

Lee et al. crosslinked chitosan using natural rubber to introduce reversible flexibility to the chitosan scaffold.[93] The crosslinking chemistry is based on a chemical reaction between the amine of chitosan and the oxirane of epoxidized natural rubber (ENR) (Fig. 3k). Different ratios of chitosan and ENR (CE73 = 7:3, CE55 = 5:5, and CE37 = 3:7) were mixed to obtain a desired mechanical toughness. As demonstrated by the peel test, CE73 showed the highest adhesive force while CE37 exhibited the lowest modulus in the stress–strain curve. However, the galvanostatic cycling test revealed that CE55 exhibited the highest capacity retention even at high current densities. The Si anode fabricated with 70 wt% SiNP (mass loading 0.6 mg cm^{-2}), 15 wt% conductive agent, and 15 wt% binder (CE55) exhibited a high capacity of 1350 mA h g^{-1} over 1600 cycles at 8 A g^{-1}. When the current density was reduced to 1 A g^{-1}, the capacity significantly increased and was maintained above 2000 mA h g^{-1} over 500 cycles. This result suggests that high adhesion strength

and low modulus of the polymer are not inevitably translated to an effective binder performance, rather a delicate balance between the two must be considered.

2.11. Carbamation

Kuo et al. prepared an in-situ crosslinked poly(ether urethane) (PEU) binder for Si anodes.[94] The crosslinking occurred by the reaction of the gallic acid (GA) crosslinker with the PEU precursors (Fig. 3l). GA contains three hydroxyl groups, which can simultaneously react with the diisocyanate groups of PEU during electrode drying, establishing a connection between three PEU chains. The Si anode was fabricated by mixing 60 wt% Si (mass loading 0.55 mg cm^{-2}), 20 wt% conductive agent, and 20 wt% binder precursors together with the crosslinker. Compared to the anode with non-crosslinked PEU, the Si anode with crosslinked PEU exhibited better cycling stability. Although the initial charge capacity and columbic efficiency of the electrodes with both crosslinked and non-crosslinked binders were similar, the electrode with the non-crosslinked binder declined gradually, while the electrode with the crosslinked binder showed a higher retention capacity (71%) over 100 cycles.

2.12. Copolymerization

Following the reports of Han et al. (section 2.3), Aoki et al. studied crosslinked PAA for a similar system with a different crosslinker.[95] Instead of carbodiimide, they employed diallyl ether crosslinker for ex-situ crosslinking (Fig. 3m). To form crosslinked poly(acrylic acid) (CLPAH) binder, acrylic acid was polymerized with different amounts of diallyl ether (0–0.7 mol%). The galvanostatic cycling test of the Si/Gr anodes with 10 wt% binder showed that moderately crosslinked 10CLPAH (0.07 mol% crosslinker) can effectively retain the initial capacity due to balanced viscosity and good mechanical durability of the crosslinked network. While the densely crosslinked 100CLPAH responded poorly to volume changes due to the lack of free carboxylic moieties and inadequate fluidity to adhere and cover the active material surface. When the crosslinked binders were neutralized before testing, the capacity and capacity retention of the corresponding anodes were significantly improved. This increase might have been evolved from the surface modification that gave rise to a stable SEI and stretched conformation of the binder due to strong ion-dipole interactions.

2.13. Photo-crosslinking

Park et al. developed a benzophenone (BP)-functionalized PAA binder by a photo-crosslinking method (Fig. 3n).[96] While most research groups have focused on thermal crosslinking, this is the first report on employing UV light to generate a network binder for the Si anode. The photoreactive BP moiety of PAA-BP was irradiated with UV light (365 nm) to generate biradical species that can extract a proton from an adjacent PAA backbone and form a connection between them. To afford crosslinked electrodes, the carbon-coated SiNP electrode with 80 wt% active materials, 10 wt% conductive agents, and 20 wt% PAA-BP was exposed to UV light. The resultant electrode exhibited a substantially enhanced capacity retention over 100 cycles and good rate capability (1420 mA h g^{-1} at 20 A g^{-1}), as compared to the anode with the un-crosslinked PAA-BP. In addition, the photo-crosslinked PAA-BP could limit the volume expansion to 38% even after full lithiation, while the bare PAA-BP electrode expanded by 63%. These results demonstrate that the photo-crosslinked network is effective in reducing the deformation as well as maintaining the electrical contacts. However, this method may be limited in thick electrodes due to the insufficient penetration depth of UV light.

2.14. In-situ polymerization

While the pre-synthesized polymers are designed to reinforce the adhesive forces with active materials through some functional groups, one of the challenges includes agglomeration in the solvent, resulting in high viscosity of slurry.[97] Consequently, homogeneous mixing of the electrode slurry may be difficult to achieve, which would worsen the interactions between binders and active materials. In-situ polymerization can be a potential approach to resolve the solubility and homogeneity issues.

Wang group proposed a facile approach employing 'chemical mixing' technique.[97] The technique involved the one-pot mixing of starting materials in the slurry including ball milled Si: carbon black (CB), binder precursors (i.e., a solution of acrylic acid monomer and ammonium peroxide initiator) and thickening agent (i.e., alginate) followed by in-situ polymerization to afford a homogeneous dispersion of active materials embedded in a binder network. The micron-sized Si electrode with only 10wt% of the binder exhibited fine microstructure and high retention capacity (80%) after several cycles compared to similar electrode with pre-formed polymer binder. The improved performance of the chemically-mixed electrode was attributed to the uniform networks of the PAA chains resulting in elevated interactions with the Si particles.

Park et al. further demonstrated this approach to construct electrodes containing PAAm hydrogel binder with mesh-like structure.[98] The Si electrode containing hydrogel binder was fabricated by mixing aqueous solutions of acrylamide monomer, initiator (ammonium persulfate), catalyst (tetramethyl ethylenediamine) and crosslinker (methylene bisacrylamide, MBAA) with SiNPs and functionalized CB (f-CB), followed by in-situ polymerization. Exploiting the in-situ approach mitigated the fabrication problems of gel-polymer electrode and was effective for the uniform distribution of SiNPs and f-CB in the gel binder without the loss of binder functionality. The resultant electrode displayed good cycling performance (1526 mA h g^{-1}) even after 500 cycles under optimum crosslinking density.
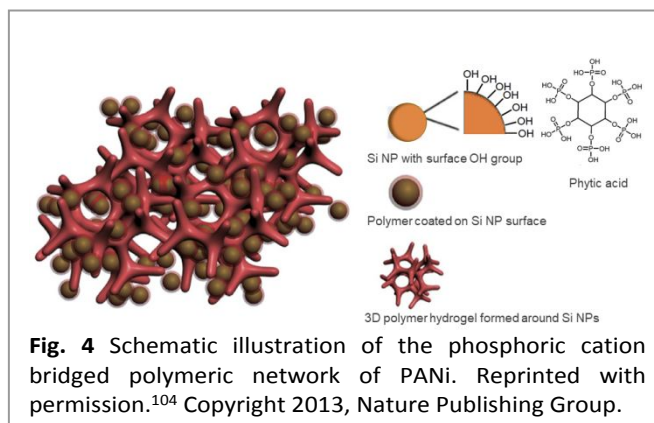
Liu et al. used a similar in-situ approach to construct a 3D interpenetrating binder network (IBN), by first swelling PVA with a furfuryl alcohol (FA) monomer, and subsequently polymerizing FA in the presence of the electrode components.[99] The IBN network constructed by interweaving hard poly(furfuryl alcohol) (PFA) and soft PVA polymers significantly improved the mechanical strength of the binder. The corresponding anode delivered significantly higher areal capacity (>10 mAh cm^{-2}) and demonstrated high energy density (>300 Wh kg^{-1}) in a full cell.

3. Physically crosslinked binders

Non-covalent crosslinking through strong supramolecular interactions of the polymer chains is one of the ideal strategies to realize the concept of simultaneous adhesion and self-healing of binders. Supramolecular interactions are rather weak in comparison to covalent bonds; however, their long-range force and inherent reversibility facilitate stronger adhesion and bond recovery by dissipating stress. These abilities rely on the strength of the supramolecular interactions. While the van der Waals interaction of PVDF is insufficient to restore the dissociated bonds under mechanical stress,[76,100-102] strong physical interactions (e.g. hydrogen bonding, ion-dipole interaction, and coordination bonding) can recover dissociated bonds more effectively.[63,103] The binders including physical crosslinking interactions are listed in Table 2.

3.1 Ionic crosslinking

Non-metal cation bridges

Fig. 4 Schematic illustration of the phosphoric cation bridged polymeric network of PANi. Reprinted with permission.[104] Copyright 2013, Nature Publishing Group.

Cui et al. developed a nanostructured conductive hydrogel binder by in-situ oxidative polymerization of polyaniline (PANi) and phytic acid.[104] The phytic acid contains six phosphoric acid groups, which can act as both gelator and crosslinker to connect with the aniline chains by protonating the amine groups of PANi (Fig. 4). The Si anode fabricated with 70 wt% SiNPs and 30 wt% binder (Si mass loading 0.2–0.3 mg cm^{-2}) retained a stable capacity (1600 mA h g^{-1}) over 1000 cycles. The improved cycle life of SiNP-PANi can be ascribed to the following reasons: (i)

Table 2 Summary of physically crosslinked binders reviewed herein. For structures, please see the discussion part or the relevant references.

Binder	Anode (mass loading in mg cm^{-2})	Crosslinking interaction	Specific capacity (mA h g^{-1})	Binder content (wt%)	Capacity retention	Ref
PANi	Si = ~60 nm (0.2−0.3)	Ionic crosslinking by non-metallic cation	~600	25	91% at 5000th cycle at 6 A g^{-1}	104
Na-Alg/Ca^{2+}	Si/C = 8/2, Si = ~100 nm (not mentioned)	Electrostatic crosslinking using divalent cations	2214	29	82.3% after 120 cycles at 0.4 A g^{-1}	106
	Si = ~200 nm (1.0−1.1)		3292	15	86% at 200th cycle at 0.4 A g^{-1}	108
Na-Alg/Ni^{2+}	Si = ~100 nm (0.45)		~ 3500	15	99.2% at 200th cycle at 0.84 A g^{-1}	109
PAA-PBI	Si/Gr=3/7 (0.8)	Reversible acid-base interaction	1376.7	10	55% after 100 cycles at 0.13 A g^{-1}	110
PAA-PEGBI	Si (0.7–0.91)		~2000	10	61% at 50th cycle at 1 A g^{-1}	111
PAA/PANI /IPN	Si = 200 nm (1.0)	Ionic interaction of cationic and anionic functionalities and covalent crosslinking using NMBA	~4100	40	2205 mA h g^{-1} after 300 cycles at 0.4 A g^{-1}	112
β-CD/6AD	Si = ~50 nm (~0.8)	Host-guest interaction	~1600	20	90% after 150 cycles at 1.5 A g^{-1}	113

hydrogen bonding between the phosphoric acids in the phytic acid with the hydroxyl groups of the Si surface, (ii) electrostatic interaction of the negatively-charged Si surface with the positively-charged PANi-doped phytic acid, (iii) the nanoporous structure of the hydrogel binder that helps the Si anode to accommodate severe volume changes and facilitates a continuous 3D conduction pathway for electrons.

Metal-cation bridge

Alginate, a natural polysaccharide has been subjected to extensive research in the field of regenerative skins and tissue scaffolds.[105] The α-L-guluronic acid (G) units of alginate can undergo ionic crosslinking with divalent cations such as Ca^{2+} to form an egg-box structure as shown in Fig. 5a. Liu et al. prepared an alginate hydrogel binder by crosslinking Na-alginate (Na-Alg) with Ca^{2+} ions for Si/C composite anodes (80:20 by weight).[106] The hydrogel binder was prepared by adding Na-Alg solution to a CaCl$_2$ solution. The Si/C composite anode constructed with 53
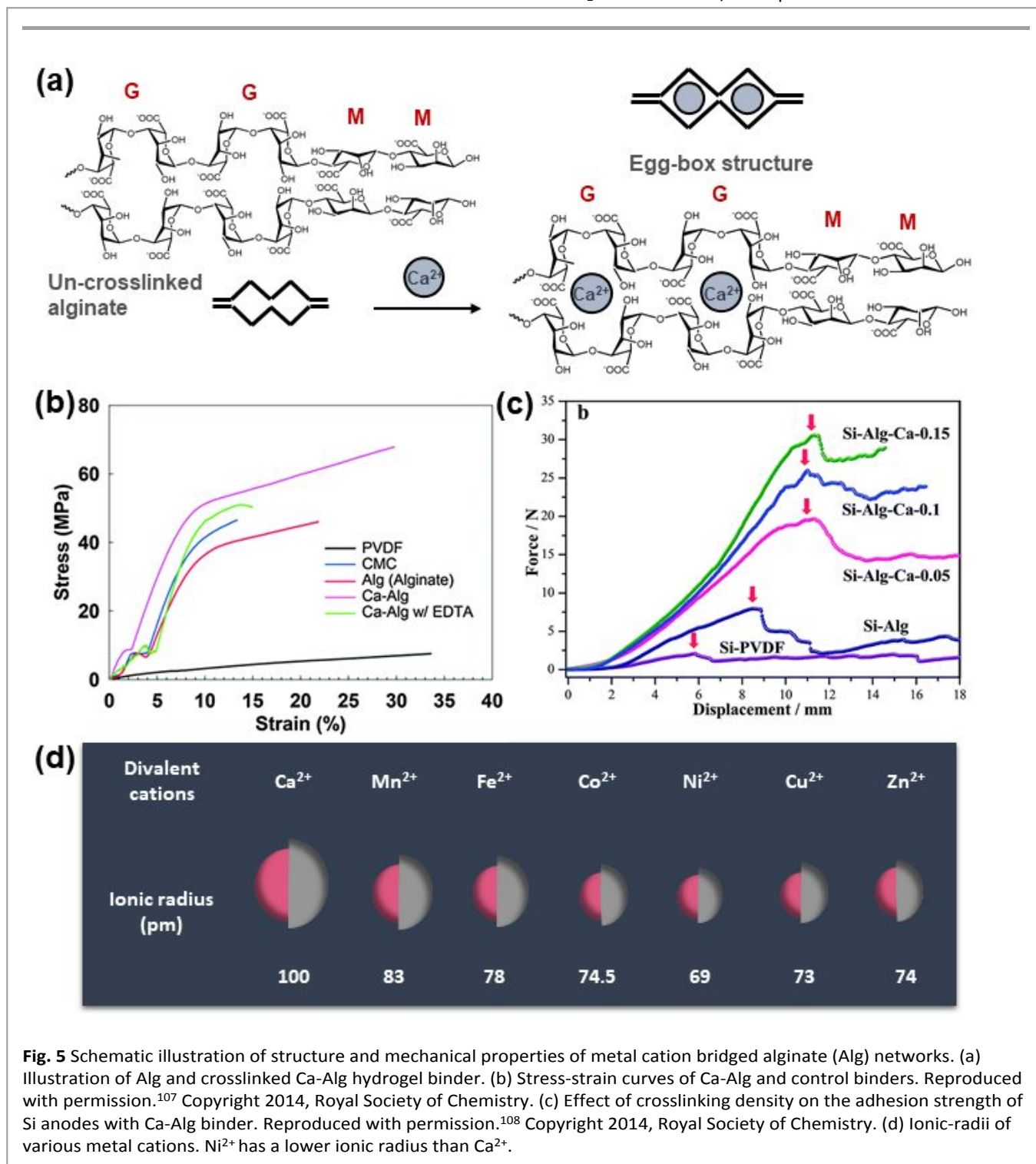

Fig. 5 Schematic illustration of structure and mechanical properties of metal cation bridged alginate (Alg) networks. (a) Illustration of Alg and crosslinked Ca-Alg hydrogel binder. (b) Stress-strain curves of Ca-Alg and control binders. Reproduced with permission.[107] Copyright 2014, Royal Society of Chemistry. (c) Effect of crosslinking density on the adhesion strength of Si anodes with Ca-Alg binder. Reproduced with permission.[108] Copyright 2014, Royal Society of Chemistry. (d) Ionic-radii of various metal cations. Ni^{2+} has a lower ionic radius than Ca^{2+}.

wt% active material, 18 wt% conductive carbon, and 29 wt% hydrogel binder showed superior cycling performance in comparison to the Si/Alg anode, with a capacity retention of 82% over 120 cycles. This was exclusively due to the enhanced mechanical strength after crosslinking.

The origin of the mechanical property enhancement of the Ca^{2+} mediated alginate binders (Ca-Alg) was carefully examined by Yoon et al.[107] They initially evaluated the electrolyte uptake of the alginate films along with CMC and PVDF. The Ca-Alg film exhibited a much lower adsorption value (~4.2%) than the controls (Na-Alg ~8.7%, CMC ~8.8%, and PVDF ~165%). The mechanical properties of the binders were also evaluated in the presence of electrolytes. The tensile test results of the Na-Alg and Ca-Alg films with adsorbed electrolytes showed that the Ca-Alg film exhibited twice the toughness (13.5 MJ m^{-3}) and four times the elastic modulus (510 MPa) compared to those of the Na-Alg film. The control experiment using ethylenediaminetetraacetic acid (EDTA) treatment revealed that the main cause of the superior mechanical strength of the Ca-Alg binder is the high un-zipping energy of the egg-box crosslinked structure, which is lost as a result of calcium captured by EDTA. Due to the robust crosslinked structure, the Ca-Alg film also exhibited enhanced strain recovery (~65% at a 5% loading strain) even after 20 cycles, while the control binders failed to pass 3 cycles (Fig. 5b). As a result, the Si anode with 10 wt% Ca-Alg binder (mass loading 0.4–0.5 mg cm^{-2}) achieved good capacity and rate capability (1029 mA h g^{-1} at 2 A g^{-1}) and maintained 83% capacity over 300 cycles. However, the preparation of a homogeneous slurry was challenging due to the rapid gelation of Alg and the metal ions.

The mechanical strength of the Ca-Alg hydrogel binder was modulated by varying the molar fraction of Ca^{2+} in the binder as reported by Zhang et al.[108] The Si anodes were fabricated using 70 wt% Si sub-microparticles (SiSMPs) (mass loading 1.0–1.1 mg cm^{-2}), 15 wt% conductive agent, and 15 wt% Ca-Alg binders (Ca^{2+} molar fraction = 0.05–0.15). The peel test results indicated that the adhesion strength of the Ca-Alg binder showed a linear dependence with the amount of $CaCl_2$ addition. As demonstrated in Fig. 5c, a stronger adhesion was achieved at higher Ca^{2+} contents due to an increase in the crosslinking density of the alginate chains. All the Si-Ca-Alg electrodes exhibited improved cyclability, and the trend in capacity retention was analogous to the peel strength (i.e., Alg-Ca-0.15 > Alg-Ca-0.1 > Alg-Ca-0.05 > Alg). However, Alg-Ca-0.15 displayed a lower ICE of 80.2% compared to those of Alg-Ca-0 (86.1%), Alg-Ca-0.05 (85.9%), and Alg-Ca-0.1 (83.2%).

Electrostatic crosslinking of alginate binders using transition metal cations was explored by Gu et al.[109] It is well known that alginate chains can be easily crosslinked by divalent cations, such as Ca^{2+}, Fe^{2+}, Cu^{2+}, and Ni^{2+}. However, the role of these cations on the mechanical strength of the crosslinked network and formation of SEI are quite different. The cycling stability of the Si anode was remarkably high when Cu^{2+} or Ni^{2+} bridged alginate binders were used. This is due to the difference in bonding strength when the alginate chains interact with various divalent cations. The Ni^{2+} ion, being the smallest cation, can form strong ionic bonds with Alg, as compared to the rest of the

cations. Consequently, a more robust network structure generated from the Ni-Alg binder provided long-term cyclability.[70] Despite Ni^{2+} exhibiting superior performance compared to Ca^{2+} in bridging the alginate chains, Ni^{2+} bridged alginate binders are less appealing for binder applications due to the high cost and toxicity.

3.2. Reversible acid-base interaction

Lim et al. exploited reversible acid-base interactions to introduce ionic crosslinks between PAA and the poly(benzimidazole) (PBI) chains.[110] The nitrogen atom in the imidazole of PBI can accept protons from the carboxylic acid groups of PAA to produce an imidazolium carboxylate pair (Fig. 6a). The ionic interaction increased the adhesive force of the PAA-PBI binder evidenced by the peel test results. As a consequence, the Si/Gr (3:7) anode fabricated with 80 wt% active material (mass loading 0.8 mg cm^{-2}), 10 wt% conductive agent, and 10 wt% PAA-PBI binder exhibited enhanced cycling performance compared to Si/Gr-PAA. PAA-PBI-2 (2 wt% PBI) showed the highest capacity (1377 mA h g^{-1}) and coulombic efficiency (average CE = 99.1%) due to the low polarization, reversible bonding, and strong adhesion. However, PAA-PBI with 5 wt% PBI crosslinker (PAA-PBI-5) weakened the adhesion of the binder to Si and decreased the electrochemical performance.

To improve processability and achieve high loading levels, the same group modified the PAA-PBI binder by introducing poly(ethylene glycol) (PEG) into PBI (PEGPBI) (Fig. 6b).[111] Notably, the anodes with the modified binders exhibited a higher initial capacity due to the decreased resistance by the ion-conducting PEG group. The Si anode with PAA-PEGPBI-2 (2 wt% PEGPBI) displayed superior adhesion and cycling capacity (1221 mA h g^{-1} after 50 cycles) compared to PAA and the control binders with higher or lower crosslinking density. These results indicate that an optimum crosslinking density between PAA and modified or unmodified PBI exists because excess crosslinking
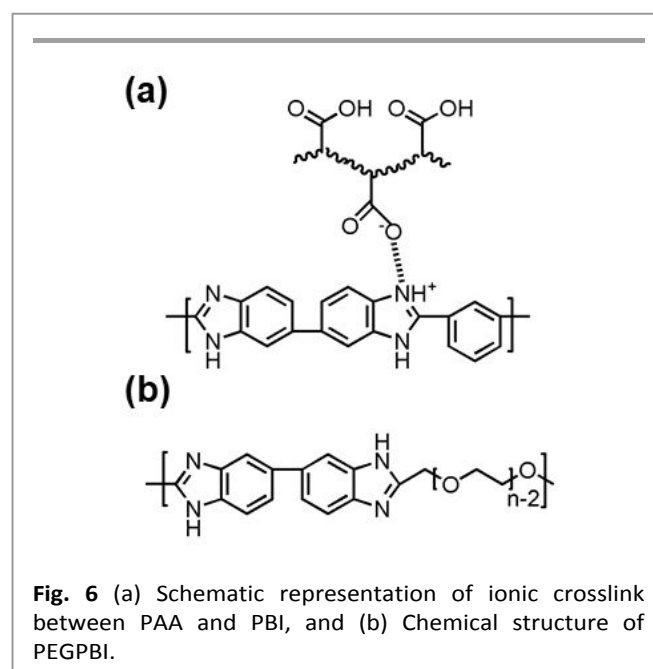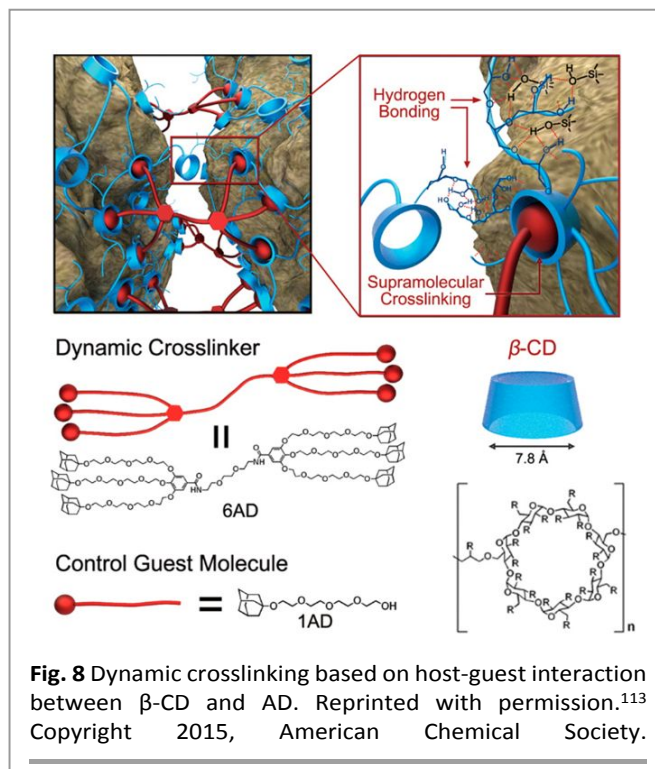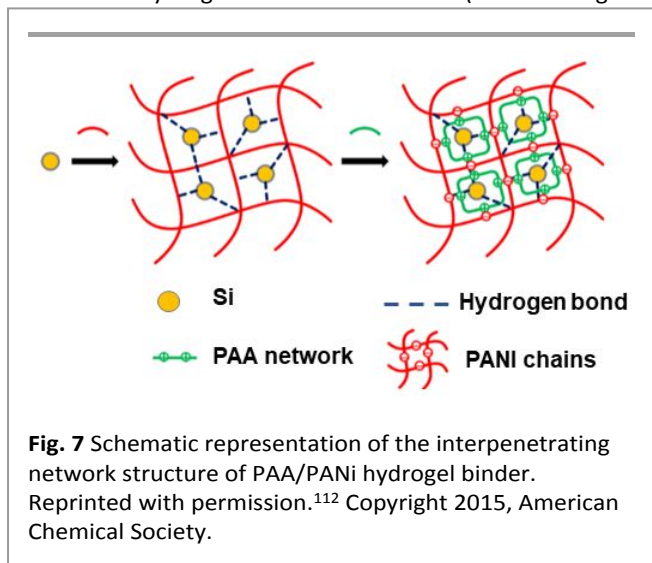

Fig. 6 (a) Schematic representation of ionic crosslink between PAA and PBI, and (b) Chemical structure of PEGPBI.

reduces the number of free carboxylic acid groups for interacting with the Si surface. Excellent adhesion to the Si surface and ionic interactions between the chains are equally important, and PAA-PEGPBI could demonstrate both properties through hydrogen bonding and acid-base interactions.

Polymeric binders that can conduct electrons is beneficial because the fraction of conductive additives in Si anodes can be reduced. Xu et al. developed a PANi incorporated PAA hydrogel binder with an interpenetrating network (IPN) and porous structure by hydrogelation of acrylic acid using *N, N'*-methylene bisacrylamide (NMBA) followed by in-situ polymerization with aniline (Fig. 7).[112] During this process, the NH_3^+ ions in PANi electrostatically interacted with the COO^- anions in PAA. The mechanical integrity of IPN and its role in adhering the Si particles was revealed by the peel test. The Si-PAA/PANi IPN electrode demonstrated an initial peel force of ~16 N, which was much higher than those of Si-PAA (~7 N) and Si-PVDF (~2 N). Consequently, Si-PAA/PANi IPN (Si:binder = 60:40) exhibited a more stable capacity after 300 cycles, unlike the Si-PAA and Si-PVDF binders. This enhanced performance of the Si anode with PAA/PANi IPN can be explained by the synergistic effect of the binder. While IPN and strong hydrogen-bonding interactions with the Si particles promoted the formation of a stable SEI film, the conducting property of the PANi chains effectively reduced the charge-transfer resistance, and the porous structure facilitated effective Li–ion transportation.

3.3. Host–Guest interaction

Kwon et al. introduced a new strategy to develop dynamically crosslinked binders for Si anodes based on host-guest interactions.[113] They demonstrated that hyperbranched cyclodextrin polymers (β-CDp) can be strongly and reversibly crosslinked by a gallic acid derived dendritic crosslinker incorporating six adamantane units (6AD) (Fig. 8). The choice of β-CD and AD as the host–guest pair rests on their strong affinity and selectivity toward each other. The crosslinking density was optimized with the β-CD/6AD ratio at 1:0.5, while an increase or decrease of 6AD resulted in an impaired cycling performance due to the dead occupancy of either host or guest in the anode. Galvanostatic cycling tests of the SiNP anode (mass loading ~0.8
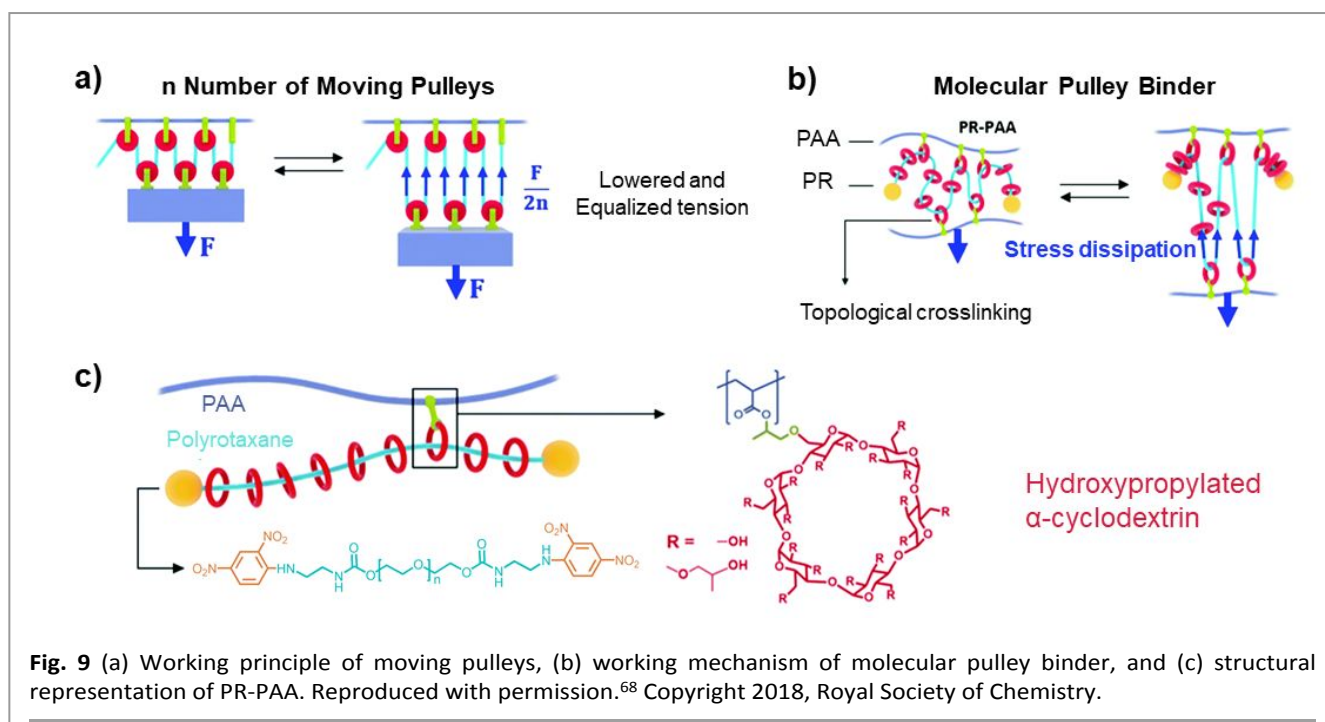

Fig. 7 Schematic representation of the interpenetrating network structure of PAA/PANi hydrogel binder. Reprinted with permission.[112] Copyright 2015, American Chemical Society.

Fig. 8 Dynamic crosslinking based on host-guest interaction between β-CD and AD. Reprinted with permission.[113] Copyright 2015, American Chemical Society.

mg cm^{-2}) with 20 wt% β-CD/6AD exhibited the highest capacity retention (90% over 150 cycles) when compared to the performance of the controls with other combinations of binder (α or γ forms of CD) and crosslinker (6AD or 1AD). The enhancement in the cycling performance of Si- β-CDp/6AD was attributed to the strong affinity and size compatibility between the host-guest pair, the appropriate length of crosslinker, and the dynamic nature of crosslinking.

4. Topologically crosslinked binders

Topological polymers such as polyrotaxane (PR) are well known for their distinctive mechanical properties due to the presence of sliding rings that act as movable crosslinks. PR is a supramolecule having a structure similar to a necklace, where, for example, (un)functionalized cyclodextrins (CD) are threaded onto a poly(ethylene glycol) chain with bulky molecular stoppers at both ends. The ring components of PR are freely movable across the axle, proving good stress-relaxing ability. Such dynamic feature of the PR has been exploited to create unique stimuli responsive materials[114,115] and molecular machines.[116,117]

Choi research group integrated the dynamic nature of PR into a binder design and developed highly elastic network binder by chemically linking PAA and the CDs of PR as shown in Fig. 9.[118] Although the connection between the polymer entities (PR and PAA) are purely covalent, the entire binder network demonstrated dynamic features due to the sliding motion of the crosslink points. Owing to the molecular pulley effect of PR, the stress generated in the binder during cycling could be uniformly distributed across the networks rather than concentrating on a particular site. Consequently, the PR-PAA binder could

Fig. 9 (a) Working principle of moving pulleys, (b) working mechanism of molecular pulley binder, and (c) structural representation of PR-PAA. Reproduced with permission.[68] Copyright 2018, Royal Society of Chemistry.

accommodate larger stresses without breakage, which was effective for maintaining the integrity of the SiMP anode by preventing the active materials from disintegration and detachment from the current collector. The benefit of topological crosslinking was clearly demonstrated in the cycling performance of the electrode consisting of 80 wt% SiMPs (mass loading 1.07 mg cm^{-2}), 10 wt% conductive agents, and 10 wt% binder. The unique binder design assisted the SiMP anode to exhibit a high areal capacity up to 150 cycles with 91% capacity retention. Despite a low binder content (10 wt%), substantial capacity retention for prolonged cycles opened a new horizon for the binder design.

Recently, the same group utilized PR-PAA supramolecular network for carbon-coated SiO$_x$ as well.[119] In this work, the surface of the carbon-coated Si particles was functionalized with hydroxylated-pyrene to enable robust interactions with the binder as well as the current collector. The complete exploitation of the sliding effect of the supramolecular binder together with the π-π and hydrogen bonding interactions between the electrode components resulted in enhanced cycling performance and capacity retention in both half-cell (92.6% in 250th cycle) and full cell (82.5% after 150 cycles) settings.

5. Self-healing binders

Self-healing binders are extensively explored to enhance the cycling stability of Si anodes. Different types of self-healing polymers including covalent and supramolecular interactions have been applied to battery technologies (Table 3).

5.1. Self-healing binders based on dynamic crosslinking

The majority of the self-healing binders for LIBs developed so far have exploited dynamic non-covalent interactions (i.e., supramolecular interactions). Although dynamic covalent

bonds such as disulfide bridges, alkoxy-amine bonds, Diels-Alder adducts, hydrazine bonds, and boronic ester linkages can be harnessed for the creation of self-healing materials,[120] non-covalent supramolecular interactions including hydrogen bonding, host-guest interactions, metal coordination bonding, and electrostatic interactions have been preferred in complex engineering systems such as batteries because the formation and reformation of non-covalent bonds is an energy-efficient process (i.e., easy to dissociate-associate).[70,121] The dynamic bonds can be formed between the binder and the active material and/or between the polymer chains. In this review, we focus on the interchain dynamic bonds between the polymer chains.

5.1.1 Self-healing based on hydrogen bonding

(i) Single hydrogen-bond

Among the various non-covalent bonds, hydrogen bonds (H-bonds) are particularly important due to two reasons: (i) most of the binders have polar functional groups, which can act as either hydrogen donor or acceptor and (ii) they can repeatedly and autonomously heal at relatively low temperatures such as room temperature.

Hu et al. developed a conductive hydrogel binder (ESVCA) with fast self-healing ability for SiNP anodes.[122] The hydrogel binder was prepared by the gelation of a complex solution of PEDOT:PSS, PVA, and 4-carboxybenzaldehyde using ammonium persulfate (APS) followed by polymerization. APS functioned as both complexing and gelation agent to establish an interpenetrating network as shown in Fig. 10a. In this system, PEDOT:PSS was responsible for electrical conductivity, while PVA acted as the hydrogen donor to form dynamic H-bonds with the sulfonate groups in the PSS. Fig. 10b and 10c illustrate the stress-strain response and self-healing mechanism of the conductive hydrogel binder. The SiNP anode (mass loading 0.53 mg cm^{-2}) with a 40% hydrogel binder exhibited a higher

Table 3 Summary of self-healing (SH) binders reviewed herein. For structures, please see the discussion part or the relevant references.

Binder	Anode (mass loading in mg cm^{-2})	Self-healing strategy	Specific capacity (mA h g^{-1})	Binder content (wt%)	Capacity retention	Ref
ESVCA	Si = ~50 nm (0.53)	Single H-bond	1786	40	71.3% after 200 cycles at 0.5 A g^{-1}	122
SHP	Si = ~3 μm (0.5−0.7)	Urea H-bond	2617	43.5	80% after 90 cycles at 0.4 A g^{-1}	124
SHP/PEG	Si = 0.8 μm (0.5−0.7)	Urea H-bond	~2600	30	80% after 150 cycles at ~1.7 A g^{-1}	127
PAA-UPy	Si = 70 nm (0.4−0.6)	Quadruple H-bond	4194	20	63% after 110 cycles at 0.8 A g^{-1}	128
Fe-PDBP	Si = ~50 nm (0.7)	Metal coordination bonding	~1500	15	81.9% after 350 cycles	130
C$_{100}$	Si (0.2 mg cm^{-1})	Electrostatic attraction	~3500	20	51% after 500 cycles at 3 A g^{-1}	131
BCx-g	Si = 50 nm (0.25−2.1)	Boronic-ester linkage	> 2750 at 0.05 C	10	87.3% after 100 cycles at 0.2 C	132
PAA-P(HEA-co-DMA)	Si = 0.5-3 μm (~1)	Dual crosslinking (covalent and hydrogen bonding)	2850	10	93.8% at 220th cycle at 1 A g^{-1}	133

reversible capacity (1242 mAh g^{-1} at 2 A g^{-1} for 200 cycles) when compared to Si/PEDOT:PSS/PVA (1092 mAh g^{-1}). The results highlight the role of the network structure in maintaining the integrity of the anode even after expansion. This novel binder also exhibited a good rate capability and elevated capacity in comparison to non-crosslinked binders.

(ii) Multiple hydrogen-bonds

Multiple hydrogen bonds are prominent in constructing supramolecular networks by offering numerous interchain sites to establish reversible physical crosslink junctions. Two classes of H-bonded binders have been reported so far: urea H-bonded binders utilizing urea end-functionalized oligomers and quadruple H-bonded binders utilizing 2-ureido-4[1H]-pyrimidinone (Upy) units.

Urea hydrogen bonding

Polymers with urea end functionalities have been extensively investigated to make supramolecular binders through urea H-bonds. Cordier et al. synthesized a self-healing material consisting of multiple urea and amide bonds, which exhibited rubber-like properties and self-healing at room temperature.[123] Based on the remarkable self-healing and elastomeric properties, Bao and co-workers developed self-healing binders for Si microparticle (SiMP) anodes.[124] The self-healing polymer (SHP) (Fig. 11a) was mixed with CB (43:7 by mass) to form a composite. The working electrode was fabricated by calendaring the SiMP electrode (mass loading 0.5−0.7 mg cm^{-2}) and SHP/CB film (1:1 by wt%). The tensile tests of the SHP binder demonstrated excellent elasticity and resistance to

stress. The self-healing binder could regenerate the superficial coating after dissociation following volume expansion and therefore imparted greater stability to the Si anode. The SiMP/SHP/CB electrode retained 80% of the initial capacity (at
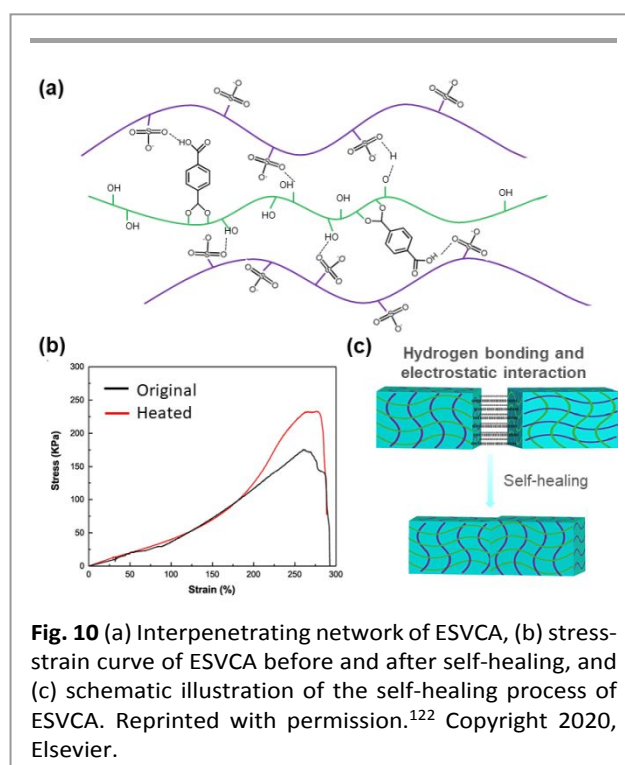

Fig. 10 (a) Interpenetrating network of ESVCA, (b) stress-strain curve of ESVCA before and after self-healing, and (c) schematic illustration of the self-healing process of ESVCA. Reprinted with permission.[122] Copyright 2020, Elsevier.
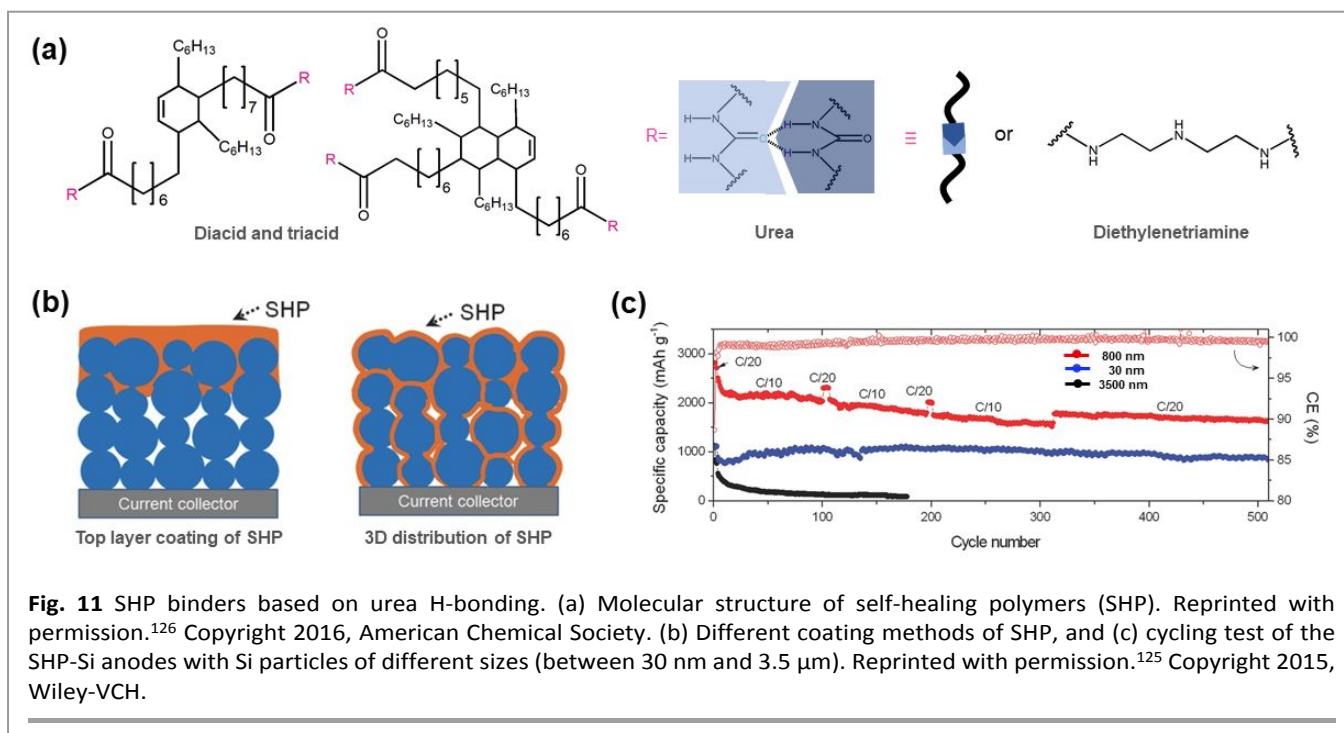
Fig. 11 SHP binders based on urea H-bonding. (a) Molecular structure of self-healing polymers (SHP). Reprinted with permission.[126] Copyright 2016, American Chemical Society. (b) Different coating methods of SHP, and (c) cycling test of the SHP-Si anodes with Si particles of different sizes (between 30 nm and 3.5 μm). Reprinted with permission.[125] Copyright 2015, Wiley-VCH.

0.4 Ag^{-1}) after 90 cycles, which is much higher in comparison to the SiMP electrodes with traditional binders (PVDF = 14%, NaCMC = 27%, and NaAlg = 47%) at the same current density.

To achieve high areal capacity, the same group performed a 3D spatial distribution of SHP along with Si particle size control.[125] Different from the initial approach where SHP was coated on the Si particles, the new approach involved a multi-dimensional distribution of SHP to promote effective self-healing by increasing the proximity of the binder and the Si particles (Fig. 11b). The electrode was fabricated by repeatedly blading the SHP/CB composite on the SiMP anode under specific conditions (120–150 ˚C). Si electrodes with different particle sizes (with the same SHP/CB) revealed that particle size control was also essential for achieving good cycling performance. Compared to SiMPs with larger diameters (3.5 and 1.0 μm), Si particles with a diameter of 0.8 μm exhibited decreased pulverization and higher specific capacity (2620 mAh g^{-1}) with approximately 80% capacity retention even after 500 cycles

(Fig. 11c). The present system exhibited an areal capacity of 4.1 mAh cm^{-2} (mass loading 1.6 mg cm^{-2}), close to the commercial requirement.

In the follow-up study, the crosslinking density was revealed as an important parameter in determining the stretchability and flow of SHP, and consequently in the cycle life of Si anodes.[126] The viscoelastic properties of the SHP varied with the weight ratio of the trifunctional fatty acid. A higher feed ratio of the triacid content resulted in an increased crosslinking density and a higher modulus, producing a stiffer polymer network. Apparent from the galvanostatic cycling test, SHP/SiNP (0.8 μm) with the highest density of crosslinked junctions (from 70% triacid) failed to exhibit stable cycling. This demonstrated the importance of the viscoelasticity of the binder to promote flow to the fractured sites and protect the active materials from the electrolytes. The SiNP electrode containing SHP with appropriate viscoelasticity and mechanical
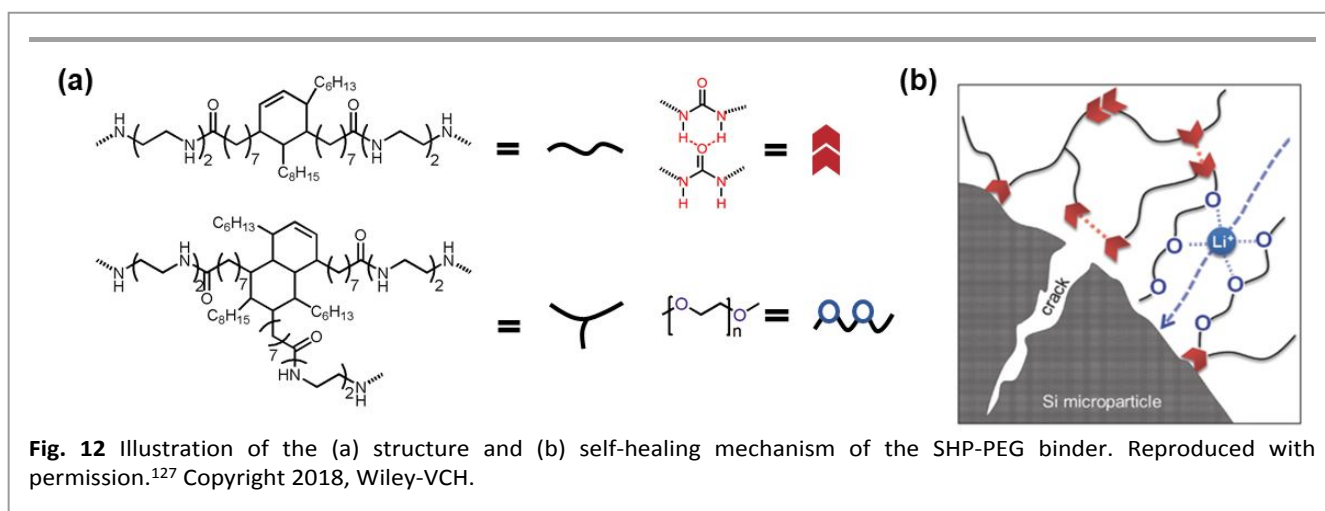

Fig. 12 Illustration of the (a) structure and (b) self-healing mechanism of the SHP-PEG binder. Reproduced with permission.[127] Copyright 2018, Wiley-VCH.

integrity (43% triacid) retained 80% capacity after 178 cycles (mass loading 0.75–1.1 mg cm^{-2}).

Ion conducting self-healing elastomeric binders prepared by introducing a portion of PEG units to SHP was reported by the same group.[127] The incorporation of a proper amount of PEG units into SHP improved the Li–ion conductivity and adhesion to Si while preserving the self-healing capability through dynamic H-bonds (Fig. 12). The SiMP/SHP-PEG anode incorporating a moderate amount (40 mol%) of oligomeric PEG side chain (MW = 750 g mol^{-1}) exhibited excellent capacity (2600 mAh g^{-1} at 0.5 C) and prolonged cycling life (up to 150 cycles) with 80% capacity retention. However, the SHP-PEG containing a longer PEG side chain (MW = 2000 g mol^{-1}) adversely affected its adhesion to Si and self-healing ability due to an increase in crystallinity and decrease in the number of urea groups.
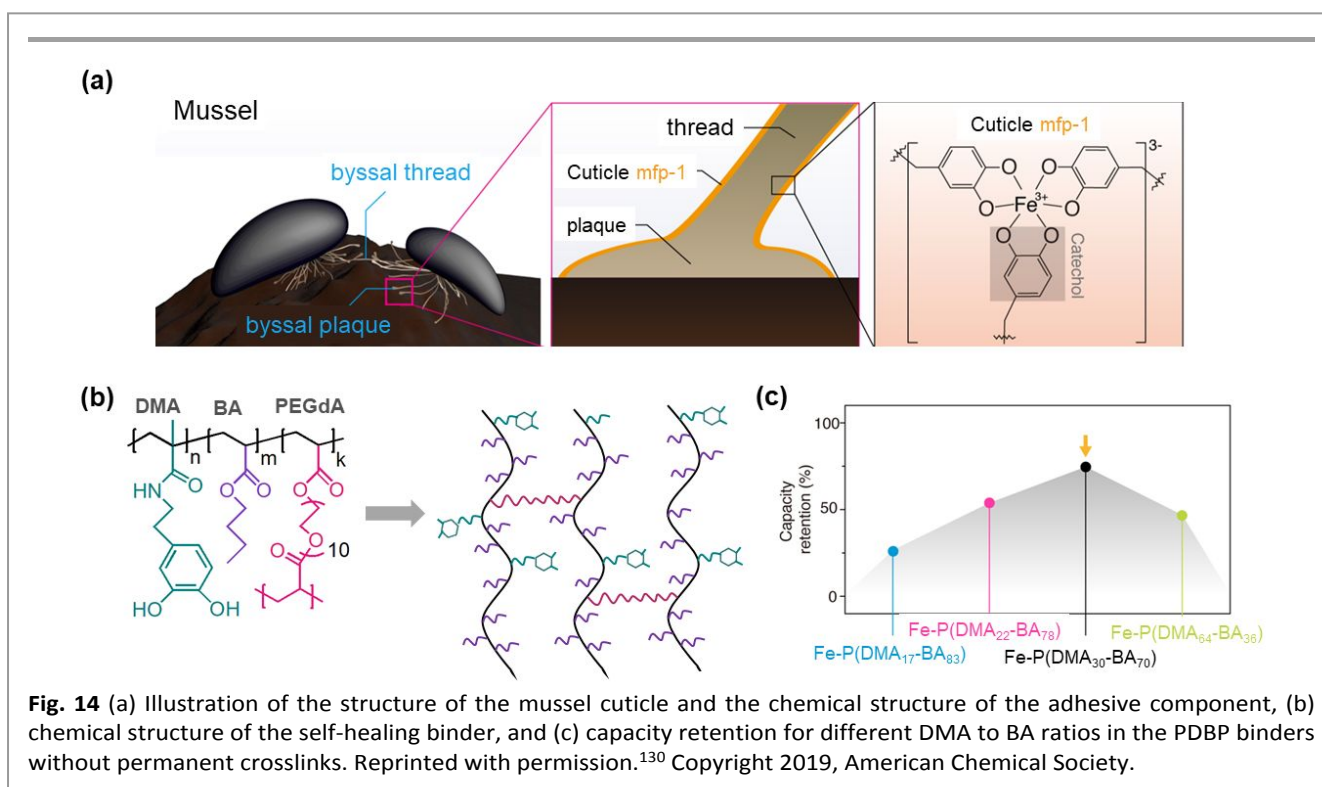
Quadruple hydrogen-bonding

Taking advantage of the ability of 2-ureido-4[1H]-pyrimidinone (UPy) derived units to dimerize in an array of quadruple hydrogen bonds, Zhang et al. reported a supramolecular binder containing UPy and PAA.[128] In contrast to single and double hydrogen bonds, quadruple hydrogen bonds have a much higher healing efficacy owing to the formation of stable dimers (Fig. 13).[129] The copolymer binder was synthesized by copolymerizing P*t*BA and UPy-HEA followed by hydrolytic cleavage of the *t*-butyl groups. With the stable yet recoverable 3D network of hydrogen bonds, the SiNP electrode (mass loading 0.4–0.6 mg cm^{-2}) with 20% binder achieved a specific capacity of 2638 mAh g^{-1} over 110 cycles, which is much higher than SiNP/PAA (1734 mAh g^{-1}) and SiNPs with other conventional binders.

5.1.2. Self-healing based on metal-ligand coordination bonds

Fig. 13 Chemical structure and illustration of the self-healing mechanism of UPy-based binders.
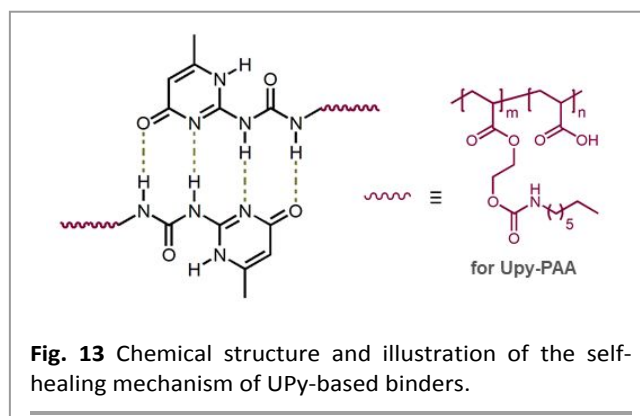
Inspired by the mussel's byssus cuticle, Choi et al. developed a metallopolymer binder with self-healing for SiNP anodes (Fig. 14).[130] In spite of the fact that the metal-ligand coordination bond is weaker than the covalent bond, the bond is strong enough to reform by the high affinity between metal and ligand. The binder was synthesized by adding a FeCl$_3$ solution to a copolymer of dopamine methacrylate (DMA, 33 mol%), butyl acrylate (BA, 66 mol%), and polyethylene glycol diacrylate (PEGDA, 1 mol%), and increasing the pH to 10. Although self-recovery after fracture evolved from the Fe^{3+} (tris)-catechol coordination crosslinks, the prolonged cycle life of the SiNP anode was due to a combined effect of the enhanced wetting by BA and permanent crosslinking by PEGDA along with the reversible coordination crosslinks. To balance the effect of each component to construct a mechanically durable binder, a set of copolymers with varying molar ratios of DMA and BA (17:83, 22:78, 30:70, and 64:36) was prepared. As shown in Fig. 13c, Si/Fe-P(DMA$_{30}$-BA$_{70}$) exhibited the highest capacity retention (74.6%) and was further used to construct Si/Fe-PDBP@pH10.

Fig. 14 (a) Illustration of the structure of the mussel cuticle and the chemical structure of the adhesive component, (b) chemical structure of the self-healing binder, and (c) capacity retention for different DMA to BA ratios in the PDBP binders without permanent crosslinks. Reprinted with permission.[130] Copyright 2019, American Chemical Society.
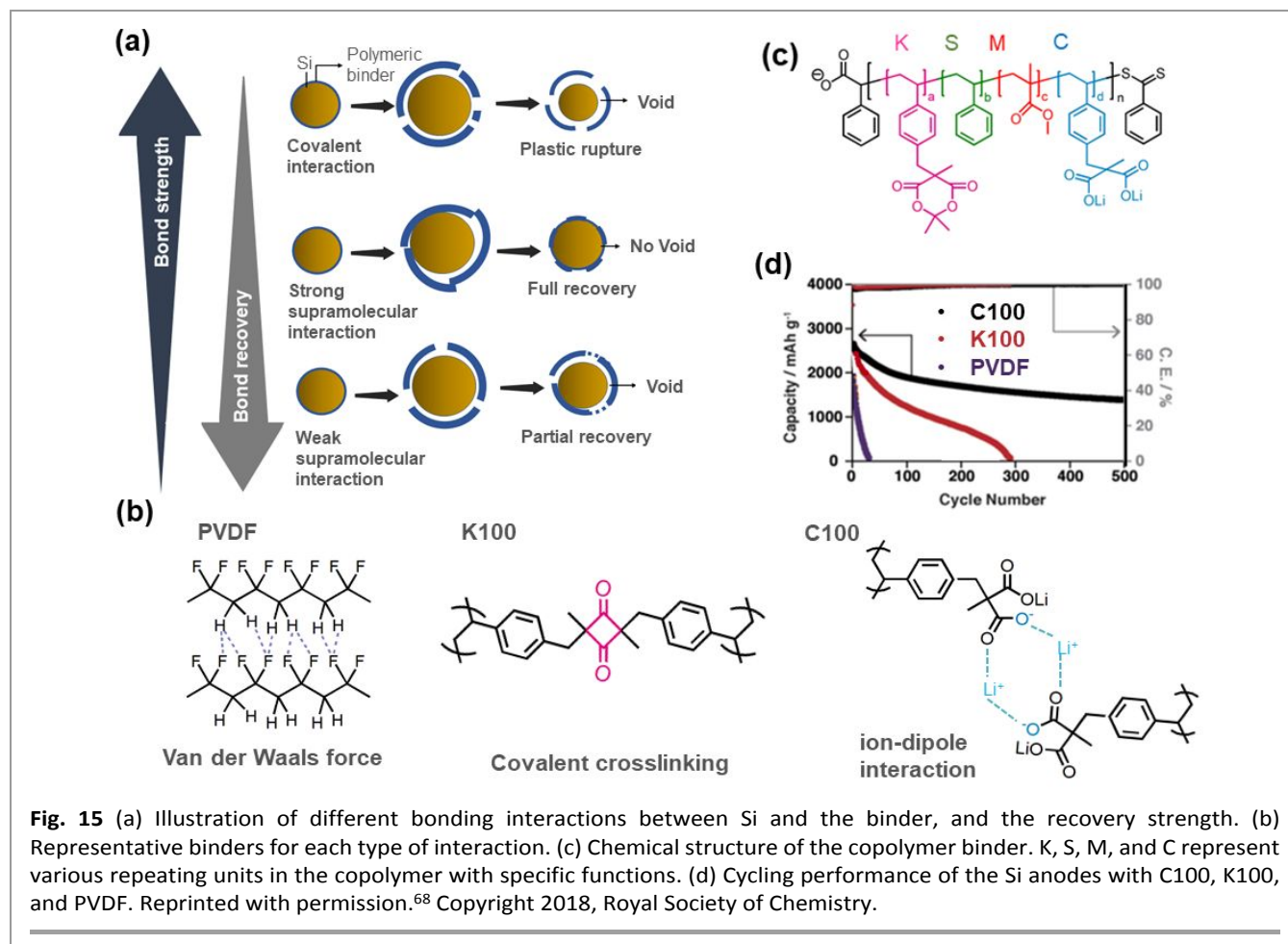
Fig. 15 (a) Illustration of different bonding interactions between Si and the binder, and the recovery strength. (b) Representative binders for each type of interaction. (c) Chemical structure of the copolymer binder. K, S, M, and C represent various repeating units in the copolymer with specific functions. (d) Cycling performance of the Si anodes with C100, K100, and PVDF. Reprinted with permission.[68] Copyright 2018, Royal Society of Chemistry.

5.1.3. Self-healing based on ion-dipole interactions

A systematic study performed by Kwon et al. on Meldrum's acid-based binders revealed the role of supramolecular interactions on the self-healing effect, which was closely associated with the reversibility of the bonding interaction.[131] Unlike covalent bonds, supramolecular interactions are intrinsically reversible and tend to dissociate under an applied force rather than rupture (Fig. 15a). Two different polymeric binders were synthesized: C_{100} with supramolecular interactions and K_{100} possessing covalent crosslinks, and their performances were compared with a PVDF binder possessing only weak van der Waals interactions (Fig. 15b). The galvanostatic cycling test of these binders showed distinct results in that the SiMP anode with C_{100} (mass loading 0.2 mg cm^{-1}, binder = 20%) had the highest capacity retention (51% over 500 cycles) owing to the self-healing effect evolved from strong ion-dipole interactions. The capacity of SiMP-PVDF rapidly dropped due to weak intermolecular forces while of SiMP-K_{100} gradually declined due to the irreversible nature of covalent bonds (Fig. 15d).

5.1.4. Self-healing based on dynamic covalent crosslinking

Ryu et al. used the dynamic covalent chemistry of the boronic ester linkages to develop a self-healing binder for both SiNP and SiMP anodes.[132] Unlike secondary covalent bonds that are less likely to re-associate after rupture, the boronic ester bonds voluntarily recover at room temperature. Among the several

polysaccharides, guar gum was chosen for crosslinking because of its larger number of hydroxyl groups compared to other polysaccharides. The crosslinker in this study was a copolymer of vinyl phenylboronic acid and vinyl functionalized poly(ethylene oxide) (PEO, MW = 950 g mol^{-1}). The boronic acid
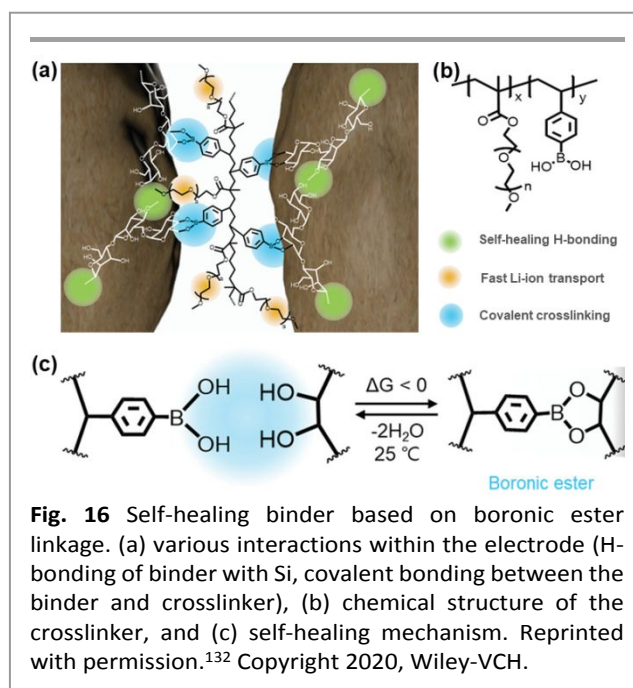

Fig. 16 Self-healing binder based on boronic ester linkage. (a) various interactions within the electrode (H-bonding of binder with Si, covalent bonding between the binder and crosslinker), (b) chemical structure of the crosslinker, and (c) self-healing mechanism. Reprinted with permission.[132] Copyright 2020, Wiley-VCH.
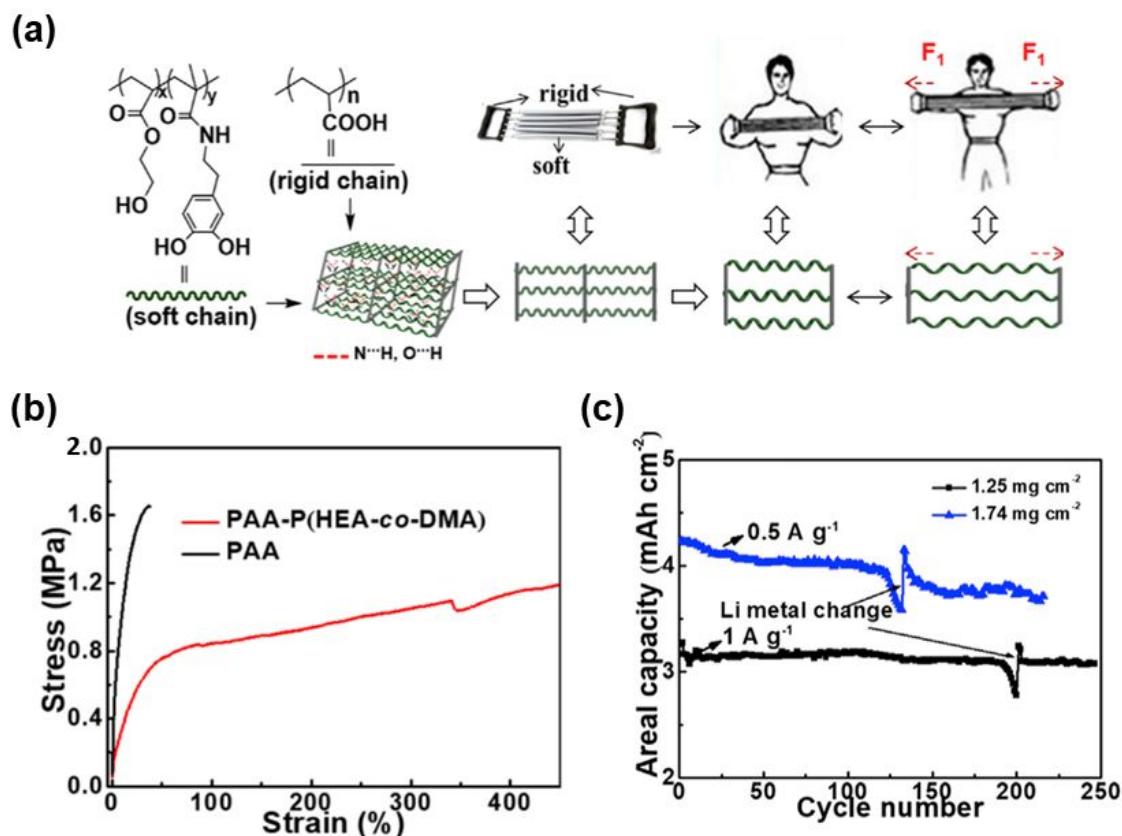
ARTICLE

Fig. 17 (a) Chemical structure and interaction of the PAA-P(HEA-co-DMA) binder and the spring expander model of the binder complex, (b) tensile tests of PAA-P(HEA-co-DMA) and PAA, and (c) Cycling performance of Si-PAA-P(HEA-co-DMA) demonstrating high areal capacity.. Reproduced with permission.[133] Copyright 2018, Elsevier.

in the crosslinker can spontaneously react with the vicinal hydroxyl groups of guar gum to generate boronic ester linkage at room temperature (Fig. 16). Moreover, the PEO in the crosslinker provides water solubility and aids Li-ion conduction. The corresponding crosslinked binder (Bc-g) showed good mechanical durability and held Si particles during stress generation. The Si anode constructed with 80 wt% SiNPs (mass loading 0.25-2.1 mg cm^{-2}), 10 wt% conductive agents, and 10 wt% binder exhibited excellent capacity retention and rate capability. Even under severe conditions (i.e., with high mass loading or with SiMP), the electrode demonstrated good cycling performance compared to the bare Guar electrode.

5.2. Self-healing binders based on dual crosslinking

A dual crosslinked binder displaying excellent cyclability and a high areal capacity for the SiMP anode was demonstrated by Xu et al.[133] The binder was an elastomer formed by an in-situ thermal condensation of PAA with a copolymer of hydroxyethyl acrylate and dopamine methacrylate P(HEA-co-DMA). The crosslinked binder PAA-P(HEA-co-DMA) was modulated by soft and rigid domains as shown in Fig. 17a. The binder exhibited significant self-healing owing to the multiple network structure and abundant local H bonds. The dual crosslinked network (i.e., covalent crosslinking between the PAA and P(HEA-co-DMA) as well as hydrogen bonds at local sites) remarkably improved the mechanical strength of the binder while the soft chains

provided good flexibility. As illustrated in Fig. 17b, PAA-P(HEA-co-DMA) can be stretched by more than 400%. In this study, a SiMP electrode with a 10 wt% PAA-P(HEA-co-DMA) binder retained 93.8% of the initial capacity at the 220th cycle (at 1 A g^{-1}), while the SiMP/PAA electrode failed to cope with the same cycling. The reported system exhibited a greater potential for practical applications by delivering a high areal capacity of 3.2 mAh cm^{-2} and good rate capability (1855 mA h g^{-1} at 5 A g^{-1}) as shown in Fig. 17c.

6. Conclusions and outlook

In this review, various chemical and physical interactions involved in the formation of network binders for Si anodes have been systematically examined. The chemistry of the polymer networks and the impact of the network binders on the mechanical properties and electrochemical performance of the electrode were highlighted. Although constituting only a small part of the electrode composition, binders play a critical role in determining the mechanical and adhesion properties of the electrode, as well as its electrochemical performance, including cycling stability and rate capability. Well-designed polymer binders, especially 3D network binders, can address the challenges of Si and other conversion-based anodes.

A broad range of polymers with abundant polar functional groups (e.g., –OH, –COOH, and -(C=O)NH$_2$) have been explored as binders for Si anodes due to the ability of these functional groups to form H-bonds and/or covalent crosslinks with the Si surface or within the polymer chains. In addition to the presence of functional groups in the binders, constructing 3D network binders often becomes critical in boosting the electrochemical performance and lifetime of Si anodes. Compared to linear binders, network binders offer multiple interaction points with the active materials, and their 3D networks are more effective in keeping the Si particles together during massive volume changes upon cycling. To this end, numerous crosslinking strategies have been employed to connect linear binders, which can be generally categorized as covalent-, physical-, and topological-crosslinking.

Covalent crosslinking, which is probably the most viable approach for industrial setting, can produce a robust chain network, and therefore is helpful for maintaining the integrity of electrode during cycling. Moreover, the covalent networks in the elastomeric binders allow the deformed polymer chains due to volume expansion of Si anode for relaxing back to their original states after the strain is released. However, the irreversible nature of covalent crosslinks is a major shortcoming when larger mechanical stresses are encountered during volume expansion. On the other hand, physically- and topologically-crosslinked binders, especially involving supramolecular interactions, offer different types of elasticity to that exhibited by covalently-crosslinked elastomeric binders due to the ability of the networks to undergo rearrangement in response to stress. Unlike covalent bonds, dynamic nature of supramolecular interactions provides reversible interchain interactions as well as binding with the Si surface, which can offer the ability to self-heal the fracture that occurs in the electrode. Although network binders having supramolecular interactions are promising to enhance long-term cycling stability of Si anodes, the difficulty in scalability and cost-issues should be addressed to extend this approach to industry.

Since the binder does not contribute to storage capacity or conductivity, the amount of the binder should be minimized, ideally below 5 wt%, just like in commercial graphite electrodes.[40] However the reduction of binder content for conversion-based anodes often leads to a poor performance due to inability to provide adequate adhesion, mechanical stability, and stable interactions with electrode components. A potential solution is to incorporate ion-conducting and/or electron-conducting moieties into binders to promote Li-ion transport and to preserve electrically conductive network by reducing the internal resistance of the cell, respectively.[127,134] Several studies investigated polymer binders with aiming to enhance ion-conductivity, however, the impact to the entire cell performance remains unclear and needs further investigation. On the other hand, electron-conducting polymer binders have shown a clear promise since electron-conducting properties can be helpful to increase mass loading and a weight ratio of "active" materials to "inert" materials in the electrode.[135] However, the enhancement of such properties in binders often sacrifice the other properties such as mechanical and adhesion

properties. Ion-conducting polymers tend to swell in electrolytes and most of conducting polymers do not provide sufficient flexibility or adhesion due to their brittleness. In reality, a single polymer binder cannot meet all the requirements of the Si anode, therefore a rational design incorporating multiple functionalities would be inevitable. 3D network binders can provide a path for such multi-functionality. The synthesis of copolymers or polymer blends with tailored molecular architecture, compositions, and functionalities to form 3D network that can manifest adhesion, mechanical strength, flexibility, conductivity, and self-healing in a synergistic way will be an ideal strategy.[136]

Despite considerable advances in the development of polymeric binders, the commercialization of Si anodes is impeded by various challenges and unmet goals. First, most of the binder systems reported to date have been evaluated only for half cells, which limits the investigation of the stable voltage window to a narrow range. For a critical evaluation of the binder and its effect on the cycle life, electrochemical tests must be performed in full cells at harsh conditions (temperatures above and below room temperature) for longer periods. Second, a majority of these binders were associated with SiNP electrodes, but further investigations on SiMP or Si/Gr composite electrodes need to be performed, which is more practical from the industrial perspective. Third, unstable and uncontrollable growth of SEI during cycling is detrimental for long-term stability of Si anode. Therefore, in-depth analysis of the effect of different polymer binders with effectual electrolyte additives that could build-up thin and stable SEI layers on interphase chemistry of SEI should be established using both ex-situ and in-situ characterizations coupled with computational analysis. Finally, a proper understanding of the rheological properties of the slurry is equally important for production and subsequent commercialization. Because the viscosity of the binder solution strongly influences the ease of mixing, the coating performance, and the dispersion quality of the slurry, the properties of the binder solution (e.g., concentration and viscosity) must be optimized to obtain an electrode with a uniform distribution of components. A variety of microscopy can be utilized to examine the homogeneity of slurry after coating, uniform crosslinking of binders, and surface roughness, etc.

To realize next-generation LIBs based on Si-anodes, extensive research in polymer binder is essential from both academia and industry. Deviating from the trial-and-error approach, future research on the polymer binders should be directed to develop multifunctional 3D network binders based on the rational design principles. With the advent of data science such as machine-learning and artificial intelligence, such rational design of polymer binders may be developed in an accelerated fashion. Further establishing the structure-property relationships of 3D network binder to the mechanical and electrochemical performance will pave the path for wide utilization of Si-anodes. With the critical comments and the comprehensive picture of crosslinking chemistries depicted herein, we hope to encourage future research in these directions to attain LIBs with high energy densities and prolonged lifetimes.

Conflicts of interest

"There are no conflicts to declare".

Acknowledgement

Notes and references

1   H. Chen, M. Ling, L. Hencz, H. Y. Ling, G. Li, Z. Lin, G. Liu and S. Zhang, *Chem. Rev.*, 2018,**118**, 8936-8982.
2   M. Hu, X. Pang and Z. Zhou, *J. Power Sources*, 2013, **237**, 229-242.
3   K. Feng, M. Li, W. Liu, A. G. Kashkooli, X. Xiao, M. Cai and Z. Chen, *Small*, 2018, **14**, 1702737.
4   V. Etacheri, R. Marom, R. Elazari, G. Salitra and D. Aurbach, *Energy Environ. Sci.*, 2011, **4**, 3243-3262.
5   J. M. Tarascon and M. Armand, *Nature*, 2001, **414**, 359-367.
6   M. Li, J. Lu, Z. Chen and K. Amine, *Adv. Mater.* 2018, **30**, 1800561.
7   B. Dunn, H. Kamath and J.-M. Tarascon, *Science*, 2011, **334**, 928-935.
8   R. Schmuch, R. Wagner, G. Hörpel, T. Placke and M. Winter, *Nat. Energy*, 2018, **3**, 267-278.
9   A. Casimir, H. Zhang, O. Ogoke, J. C. Amine, J. Lu and G. Wu, *Nano Energy*, 2016, **27**, 359-376.
10   M. Ashuri, Q. He and L. L. Shaw, *Nanoscale*, 2016, **8**, 74-103.
11   N.-S. Choi, Z. Chen, S. A. Freunberger, X. Ji, Y.-K. Sun, K. Amine, G. Yushin, L. F. Nazar, J. Cho and P. G. Bruce, *Angew. Chem. Int. Ed.*, 2012, **51**, 9994-10024.
12   T.-H. Kim, J.-S. Park, S. K. Chang, S. Choi, J. H. Ryu and H.-K. Song, *Adv. Energy Mater.*, 2012, **2**, 860-872.
13   Y. Zhang, N. Du and D. Yang, *Nanoscale*, 2019, **11**, 19086-19104.
14   P. Li, G. Zhao, X. Zheng, X. Xu, C. Yao, W. Sun and S. X. Dou, *Energy Storage Mater.*, 2018, **15**, 422-446.
15   H. Wu and Y. Cui, *Nano Today*, 2012, **7**, 414-429.
16   T. Devic, B. Lestriez and L. Roué, *ACS Energy Lett.*, 2019, **4**, 550-557.
17   S. Chae, M. Ko, K. Kim, K. Ahn and J. Cho, *Joule*, 2017, **1**, 47-60.
18   V. Aravindan, Y.-S. Lee and S. Madhavi, *Adv. Energy Mater.*, 2015, **5**, 1402225.
19   P. Verma, P. Maire and P. Novák, *Electrochim. Acta*, 2010, **55**, 6332-6341.
20   A. Wang, S. Kadam, H. Li, S. Shi and Y. Qi, *Npj Comput. Mater.*, 2018, **4**.
21   W. Luo, X. Chen, Y. Xia, M. Chen, L. Wang, Q. Wang, W. Li and J. Yang, *Adv. Energy Mater.*, 2017, **7**, 1701083
22   W.-J. Zhang, *J. Power Sources*, 2011, **196**, 13-24.
23   X. Chen, H. Li, Z. Yan, F. Cheng and J. Chen, *Sci. China Mater.*, 2019, **62**, 1515-1536.
24   Y. Sun, K. Liu and Y. Zhu, *J. Nanomater.*, 2017, **2017**, 1-15.
25   E. Radvanyi, E. De Vito, W. Porcher, J. Danet, P. Desbois, J.-F. Colin and S. J. Si Larbi, *J. Mater. Chem. A*, 2013, **1**, 4956-4965.
26   H. Sitinamaluwa, J. Nerkar, M. Wang, S. Zhang and C. Yan, *RSC Adv.*, 2017, **7**, 13487-13497.
27   R. Teki, M. K. Datta, R. Krishnan, T. C. Parker, T.-M. Lu, P. N. Kumta and N. Koratkar, *Small*, 2009, **5**, 2236-2242.
28   X. H. Liu, L. Zhong, S. Huang, S. X. Mao, T. Zhu and J. Y. Huang, *ACS Nano*, 2012, **6**, 1522 1531.
29   H. Kim, M. Seo, M.-H. Park and J. Cho, *Angew. Chem. Int. Ed.*, 2010, **49**, 2146-2149.
30   J. Cho, *J. Mater. Chem.*, 2010, **20**, 4009-4014.
31   M. Ge, X. Fang, J. Rong and C. Zhou, *Nanotechnology*, 2013, **24**, 422001.
32   M. Ge, J. Rong, X. Fang and C. Zhou, *Nano Lett.*, 2012, **12**, 2318-2323.
33   X. Li, M. Gu, S. Hu, R. Kennard, P. Yan, X. Chen, C. Wang, M. J. Sailor, J.-G. Zhang and J. Liu, *Nat. Commun.*, 2014, **5**, 4105.
34   H. Kim, B. Han, J. Choo and J. Cho, *Angew. Chem. Int. Ed.*, 2008, **47**, 10151-10154.
35   N. Liu, Z. Lu, J. Zhao, M. T. McDowell, H.-W. Lee, W. Zhao and Y. Cui, *Nat. Nanotechnol.*, 2014, **9**, 187-192.
36   N. Liu, H. Wu, M. T. McDowell, Y. Yao, C. Wang and Y. Cui, *Nano Lett.*, 2012, **12**, 3315-3321.
37   Z. Lu, N. Liu, H.-W. Lee, J. Zhao, W. Li, Y. Li and Y. Cui, *ACS Nano*, 2015, **9**, 2540-2547.
38   H. Wu, G. Chan, J. W. Choi, I. Ryu, Y. Yao, M. T. McDowell, S. W. Lee, A. Jackson, Y. Yang, L. Hu and Y. Cui, *Nat. Nanotechnol.*, 2012, **7**, 310-315.
39   M. Ko, S. Chae and J. Cho, *ChemElectroChem*, 2015, **2**, 1645-1651.
40   S. L. Chou, Y. Pan, J. Z. Wang, H. K. Liu and S. X. Dou, *Phys. Chem. Chem. Phys.*, 2014, **16**, 20347-20359.
41   G. G. Eshetu and E. Figgemeier, *ChemSusChem*, 2019, **12**, 2515-2539.
42   C. C. Nguyen, T. Yoon, D. M. Seo, P. Guduru and B. L. Lucht, *ACS Appl. Mater. Interfaces*, 2016, **8**, 12211-12220.
43   Z. Liu, S. Han, C. Xu, Y. Luo, N. Peng, C. Qin, M. Zhou, W. Wang, L. Chen and S. Okada, *RSC Adv.*, 2016, **6**, 68371-68378
44   Y. Jiang, D. Mu, S. Chen, B. Wu, K. Cheng, L. Li and F. Wu, *J. Power Sources*, 2016, **325**, 630-636.
45   J. S. Bridel, T. Azaïs, M. Morcrette, J. M. Tarascon and D. Larcher, *Chem. Mater.*, 2010, **22**, 1229-1241.
46   I. Kovalenko, B. Zdyrko, A. Magasinski, B. Hertzberg, Z. Milicev, R. Burtovyy, I. Luzinov and G. Yushin, *Science*, 2011, **334**, 75-79.
47   D.-E. Yoon, C. Hwang, N.-R. Kang, U. Lee, D. Ahn, J.-Y. Kim and H.-K. Song, *ACS Appl. Mater. Interfaces*, 2016, **8**, 4042-4047.
48   Magasinski, B. Zdyrko, I. Kovalenko, B. Hertzberg, R. Burtovyy, C. F. Huebner, T. F. Fuller, I. Luzinov and G. Yushin, *ACS Appl. Mater. Interfaces*, 2010, **2**, 3004-3010.
49   H. K. Park, B. S. Kong and E. S. Oh, *Electrochem. commun.* 2011, **13**, 1051-1053.
50   S. I. Choi, Y. M. Lee, H. C. Jeong, E. J. Jung, M. S. Lee, J. Kim, Y. H. Kim and Y. S. Won, *Korean J. Chem. Eng.*, 2018, **56**, 139-142.
51   L. Luo, Y. Xu, H. Zhang, X. Han, H. Dong, X. Xu, C. Chen, Y. Zhang and J. Lin, *ACS Appl. Mater. Interfaces*, 2016, **8**, 8154-8161.
52   B. Hu, I. Shkrob, S. Zhang, L. Zhang, J. Zhang, Y. Li, C. Liao, Z. Zhang and W. Lu, *J. Power Sources*, 2018, **378**, 671-676.
53   L. Chen, X. Xie, J. Xie, K. Wang and J. Yang, *J. Appl. Electrochem.*, 2006, **36**, 1099-1104.

54   S. Huang, J. Ren, R. Liu, Y. Bai, X. Li, Y. Huang, M. Yue, X. He and G. Yuan, *New J. Chem.*, 2018, **42**, 6742-6749.

55   Y. K. Jeong, T. W. Kwon, I. Lee, T. S. Kim, A. Coskun and J. W. Choi, *Nano Lett.*, 2014, **14**, 864-870.

56   M. Ling, Y. Xu, H. Zhao, X. Gu, J. Qiu, S. Li, M. Wu, X. Song, C. Yan, G. Liu and S. Zhang, *Nano Energy*, 2015, **12**, 178-185.

57   Y. K. Jeong, T.-w. Kwon, I. Lee, T.-S. Kim, A. Coskun and J. W. Choi, *Energy Environ. Sci.*, 2015, **8**, 1224-1230.

58   L. Wei, C. Chen, Z. Hou and H. Wei, *Sci. Rep.*, 2016, **6**, 19583.

59   C. Luo, L. Du, W. Wu, H. Xu, G. Zhang, S. Li, C. Wang, Z. Lu and Y. Deng, *ACS Sustain. Chem. Eng.*, 2018, **6**, 12621-12629.

60   J.-I. Lee, H. Kang, K. H. Park, M. Shin, D. Hong, H. J. Cho, N.-R. Kang, J. Lee, S. M. Lee, J.-Y. Kim, C. K. Kim, H. Park, N.-S. Choi, S. Park and C. Yang, *Small*, 2016, **12**, 3119-3127.

61   T. Liu, Q. Chu, C. Yan, S. Zhang, Z. Lin and J. Lu, *Adv. Energy Mater.*, 2019, **9**, 1802645.

62   Y. Cai, Y. Li, B. Jin, A. Ali, M. Ling, D. Cheng, J. Lu, Y. Hou, Q. He, X. Zhan, F. Chen and Q. Zhang, *ACS Appl. Mater. Interfaces*, 2019, **11**, 46800-46807.

63   Z.-H. Wu, J.-Y. Yang, B. Yu, B.-M. Shi, C.-R. Zhao and Z.-L. Yu, *Rare Met.*, 2016, **38**, 832-839.

64   R. You, X. Han, Z. Zhang, L. Li, C. Li, W. Huang, J. Wang, J. Xu and S. Chen, *Ionics*, 2019, **25**, 4109-4118.

65   L. Wei and Z. Hou, *J. Mater. Chem. A*, 2017, **5**, 22156-22162.

66   Lee, S. Lim and T.-H. Kim, *B. Korean Chem. Soc.*, 2018, **39**, 873-878.

67   M. Tian, X. Chen, S. Sun, D. Yang and P. Wu, *Nano Res.*, 2019, **12**, 1121-1127.

68   T.-w. Kwon, J. W. Choi and A. Coskun, *Chem. Soc. Rev.*, 2018, **47**, 2145-2164.

69   Z. Wei, J. H. Yang, J. Zhou, F. Xu, M. Zrinyi, P. H. Dussault, Y. Osada and Y. M. Chen, *Chem. Soc. Rev.*, 2014, **43**, 8114-8131.

70   Y. Pan, S. Gao, F. Sun, H. Yang and P.-F. Cao, *Chem. Eur. J.*, 2019, **25**, 10976-10994.

71   A. J. R. Amaral and G. Pasparakis, *Polym. Chem.*, 2017, **8**, 6464-6484.

72   Y. Shi, X. Zhou and G. Yu, *Acc. Chem. Res.*, 2017, **50**, 2642-2652.

73   T. Li, Z.-Y. Wu, Y. Lu, Y. Zhou, Q. S. Huang, L. Huang and S. G. Sun, *Adv. Energy Mater.*, 2017, **7**.

74   B. Koo, H. Kim, Y. Cho, K. T. Lee, N.-S. Choi and J. Cho, *Angew. Chem. Int. Ed.*, 2012, **51**, 8762-8767.

75   P. Parikh, M. Sina, A. Banerjee, X. Wang, M. S. D'Souza, J.-M. Doux, E. A. Wu, O. Y. Trieu, Y. Gong, Q. Zhou, K. Snyder and Y. S. Meng, *Chem. Mater.*, 2019, **31**, 2535-2544.

76   J. Li, R. B. Lewis and J. R. Dahn, *Electrochemical and Solid St.*, 2007, **10**, A17.

77   Z. Karkar, D. Guyomard, L. Roué and B. Lestriez, *Electrochim. Acta*, 2017, **258**, 453-466.

78   T. Jeena, J.-I. Lee, S. H. Kim, C. Kim, J.-Y. Kim, S. Park and J.-H. Ryu, *ACS Appl. Mater. Interfaces*, 2014, **6**, 18001-18007.

79   J. Song, M. Zhou, R. Yi, T. Xu, M. L. Gordin, D. Tang, Z. Yu, M. Regula and D. Wang, *Adv. Funct. Mater.*, 2014, **24**, 5904-5910.

80   S. Scognamillo, V. Alzari, D. Nuvoli and A. Mariani, *J. Polym. Sci. A Polym. Chem.*, 2010, **48**, 2486-2490.

81   C. Hwang, S. Joo, N.-R. Kang, U. Lee, T.-H. Kim, Y. Jeon, J. Kim, Y.-J. Kim, J.-Y. Kim, S.-K. Kwak and H.-K. Song, *Sci. Rep.*, 2015, **5**, 14433.

82   X. Zeng, Y. Shi, Y. Zhang, R. Tang and L. Wei, *RSC Adv.*, 2018, **8**, 29230-29236.

83   S. Sun, D. He, P. Li, Y. Liu, Q. Wan, Q. Tan, Z. Liu, F. An, G. Gong and X. Qu, *J. Power Sources*, 2020, **454**, 227907.

84   T. Jeena, T. Bok, S. H. Kim, S. Park, J. Y. Kim, S. Park and J. H. Ryu, *Nanoscale*, 2016, **8**, 9245-9253.

85   Z. J. Han, N. Yabuuchi, S. Hashimoto, T. Sasaki and S. Komaba, *ECS Electrochem. Lett.*, 2012, **2**, A17-A20.

86   C. Chen, S. H. Lee, M. Cho, J. Kim and Y. Lee, *ACS Appl. Mater. Interfaces*, 2016, **8**, 2658-2665.

87   P.-F. Cao, G. Yang, B. Li, Y. Zhang, S. Zhao, S. Zhang, A. Erwin, Z. Zhang, A. P. Sokolov, J. Nanda and T. Saito, *ACS Energy Lett.*, 2019, **4**, 1171-1180.

88   X. Shan, Z. Cao, G. Zhu, Y. Wang, Q. Qu, G. Liu and H. Zheng, *J. Mater. Chem. A*, 2019, **7**, 26029-26038.

89   T. Phromsopha and Y. Baimark, *Int. J. Biomater.*, 2014, **2014**, 829490.

90   S. Chen, H. Y. Ling, H. Chen, S. Zhang, A. Du and C. Yan, *J. Power Sources*, 2020, **450**, 227671.

91   D. Lee, H. Park, A. Goliaszewski, Y.-k. Byeun, T. Song and U. Paik, *Ind. Eng. Chem. Res.*, 2019, **58**, 8123-8130.

92   J. Son, T. N. Vo, S. Cho, A. N. Preman, I. T. Kim and S.-k. Ahn, *J. Power Sources*, 2020, **458**, 228054.

93   S. H. Lee, J. H. Lee, D. H. Nam, M. Cho, J. Kim, C. Chanthad and Y. Lee, *ACS Appl. Mater. Interfaces*, 2018, **10**, 16449-16457.

94   T.-C. Kuo, C.-Y. Chiou, C.-C. Li and J.-T. Lee, *Electrochim. Acta*, 2019, **327**, 135011.

95   S. Aoki, Z.-J. Han, K. Yamagiwa, N. Yabuuchi, M. Murase, K. Okamoto, T. Kiyosu, M. Satoh and S. Komaba, *J. Electrochem. Soc.*, 2015, **162**, A2245-A2249.

96   Y. Park, S. Lee, S.-H. Kim, B. Y. Jang, J. S. Kim, S. M. Oh, J.-Y. Kim, N.-S. Choi, K. T. Lee and B.-S. Kim, *RSC Adv.*, 2013, **3**, 12625.

97   C. Li, T. Shi, H. Yoshitake and H. Wang, *J. Mater. Chem. A*, 2016, **4**, 16982-16991.

98   H. Woo, K. Park, J. Kim, A. J. Yun, S. Nam and B. Park, *Adv. Mater. Interfaces*, 2020, **7**, 1901475.

99   T. Liu, Q. Chu, C. Yan, S. Zhang, Z. Lin and J. Lu, *Adv. Energy Mater.*, 2019, **9**, 1802645.

100 N.-S. Choi, K. H. Yew, W.-U. Choi and S.-S. Kim, *J. Power Sources*, 2008, **177**, 590-594.

101 H. Huang, G. Han, J. Xie, Q. Zhang, *Int. J. Electrochem. Sci.*, 2016, **11**, 8697-8708

102 S. Komaba, N. Yabuuchi, T. Ozeki, Z.-J. Han, K. Shimomura, H. Yui, Y. Katayama and T. Miura, *J. Phys. Chem. C*, 2012, **116**, 1380-1389.

103 Y. K. Jeong, T.-w. Kwon, I. Lee, T.-S. Kim, A. Coskun and J. W. Choi, *Nano Lett.*, 2014, **14**, 864-870.

104 H. Wu, G. Yu, L. Pan, N. Liu, M. T. McDowell, Z. Bao and Y. Cui, *Nat. Commun.*, 2013, **4**, 1943.

105 C. K. Kuo and P. X. Ma, *Biomaterials*, 2001, **22**, 511-521.

106 J. Liu, Q. Zhang, Z. Y. Wu, J. H. Wu, J. T. Li, L. Huang and S. G. Sun, *Chem. Commun. (Camb)*, 2014, **50**, 6386-6389.

107 J. Yoon, D. X. Oh, C. Jo, J. Lee and D. S. Hwang, *Phys. Chem. Chem. Phys.*, 2014, **16**, 25628-25635.

108 L. Zhang, L. Zhang, L. Chai, P. Xue, W. Hao and H. Zheng, *J. Mater. Chem. A*, 2014, **2**, 19036-19045.

109 Y. Gu, S. Yang, G. Zhu, Y. Yuan, Q. Qu, Y. Wang and H. Zheng, *Electrochim. Acta*, 2018, **269**, 405-414.

110 S. Lim, S. Chu, K. Lee, T. Yim, Y.-J. Kim, J. Mun and T.-H. Kim, *ACS Appl. Mater. Interfaces*, 2015, **7**, 23545-23553.

111 S. Lim, K. Lee, I. Shin, A. Tron, J. Mun, T. Yim and T.-H. Kim, *J. Power Sources*, 2017, **360**, 585-592.

112 X. Yu, H. Yang, H. Meng, Y. Sun, J. Zheng, D. Ma and X. Xu, *ACS Appl. Mater. Interfaces*, 2015, **7**, 15961-15967.

113 T.-w. Kwon, Y. K. Jeong, E. Deniz, S. Y. AlQaradawi, J. W. Choi and A. Coskun, *ACS Nano*, 2015, **9**, 11317-11324.

114 Y. Takashima, Y. Hayashi, M. Osaki, F. Kaneko, H. Yamaguchi and A. Harada, *Macromolecules*, 2018, **51**, 4688-4693.

115 L. Zhou, J. Li, Q. Luo, J. Zhu, H. Zou, Y. Gao, L. Wang, J. Xu, Z. Dong and J. Liu, *Soft Matter*, 2013, **9**, 4635-4641.

116 Y. Qiu, B. Song, C. Pezzato, D. Shen, W. Liu, L. Zhang, Y. Feng, Q.-H. Guo, K. Cai, W. Li, H. Chen, M. T. Nguyen, Y. Shi, C. Cheng, R. D. Astumian, X. Li and J. F. Stoddart, *Science*, 2020, **368**, 1247-1253.

117 X. Hou, C. Ke, C. J. Bruns, P. R. McGonigal, R. B. Pettman and J. F. Stoddart, *Nat. Commun.*, 2015, **6**, 6884.

118 S. Choi, T.-w. Kwon, A. Coskun and J. W. Choi, *Science*, 2017, **357**, 279-283.

119 Y. Cho, J. Kim, A. Elabd, S. Choi, K. Park, T.-w. Kwon, J. Lee, K. Char, A. Coskun and J. W. Choi, *Adv. Mater.*, 2019, **31**, 1905048.

120 Y. Yang and M. W. Urban, *Chem. Soc. Rev.*, 2013, **42**, 7446-7467.

121 H. Wang, P. Wang, Y. Feng, J. Liu, J. Wang, M. Hu, J. Wei and Y. Huang, *ChemElectroChem*, 2019, **6**, 1605-1622.

122 S. Hu, L. Wang, T. Huang and A. Yu, *J. Power Sources*, 2020, **449**, 227472.

123 P. Cordier, F. Tournilhac, C. Soulie-Ziakovic and L. Leibler, *Nature*, 2008, **451**, 977-980.

124 C. Wang, H. Wu, Z. Chen, M. T. McDowell, Y. Cui and Z. Bao, *Nat. Chem.*, 2013, **5**, 1042-1048.

125 Z. Chen, C. Wang, J. Lopez, Z. Lu, Y. Cui and Z. Bao, *Adv. Energy Mater.*, 2015, **5**, 1401826.

126 J. Lopez, Z. Chen, C. Wang, S. C. Andrews, Y. Cui and Z. Bao, *ACS Appl. Mater. Interfaces*, 2016, **8**, 2318-2324.

127 T. Munaoka, X. Yan, J. Lopez, J. W. F. To, J. Park, J. B.-H. Tok, Y. Cui and Z. Bao, *Adv. Energy Mater.*, 2018, **8**, 1703138.

128 G. Zhang, Y. Yang, Y. Chen, J. Huang, T. Zhang, H. Zeng, C. Wang, G. Liu and Y. Deng, *Small*, 2018, **14**, 1801189.

129 Y. Lin and G. Li, *J. Mater. Chem. B*, 2014, **2**, 6878-6885.

130 Y. K. Jeong and J. W. Choi, *ACS Nano*, 2019, **13**, 8364-8373.

131 T. W. Kwon, Y. K. Jeong, I. Lee, T. S. Kim, J. W. Choi and A. Coskun, *Adv. Mater.*, 2014, **26**, 7979-7985.

132 J. Ryu, S. Kim, J. Kim, S. Park, S. Lee, S. Yoo, J. Kim, N.-S. Choi, J.-H. Ryu and S. Park, *Adv. Funct. Mater.*, 2020, **30**, 1908433.

133 Z. Xu, J. Yang, T. Zhang, Y. Nuli, J. Wang and S.-i. Hirano, *Joule*, 2018, **2**, 950-961.

134 V. A. Nguyen and C. Kuss, *J. Electrochem. Soc.*, 2020, **167**, 065501

135 S. Gao, F. Sun, A. Brady, Y. Pan, A. Erwin, D. Yang, V. Tsukruk, A. G. Stack, T. Saito, H. Yang and P.-F. Cao, *Nano Energy*, 2020, **73**, 104804.

136 Y. Yang, S. Wu, Y. Zhang, C. Liu, X. Wei, D. Luo and Z. Lin, *Chem. Eng. J.*, 2021, **406**, 126807.

Table of Contents

Progress of 3D Network Binders in Silicon Anodes for Lithium Ion Batteries

Anjali N. Preman[a], Hyocheol Lee[a], Jungwoo Yoo[b], Il Tae Kim[c],*, Tomonori Saito[d],* Suk-kyun Ahn[a],*